



Deposited via The University of Sheffield.

White Rose Research Online URL for this paper:

<https://eprints.whiterose.ac.uk/id/eprint/208921/>

Version: Published Version

Article:

Oleng, M., Ozdemir, Z. and Pilakoutas, K. (2024) Probabilistic seismic hazard assessment framework for Uganda: a stochastic event-based modelling approach. *Bulletin of Earthquake Engineering*, 22 (5). pp. 1539-1579. ISSN: 1570-761X

<https://doi.org/10.1007/s10518-024-01856-6>

Reuse

This article is distributed under the terms of the Creative Commons Attribution (CC BY) licence. This licence allows you to distribute, remix, tweak, and build upon the work, even commercially, as long as you credit the authors for the original work. More information and the full terms of the licence here:

<https://creativecommons.org/licenses/>

Takedown

If you consider content in White Rose Research Online to be in breach of UK law, please notify us by emailing eprints@whiterose.ac.uk including the URL of the record and the reason for the withdrawal request.



Probabilistic seismic hazard assessment framework for Uganda: a stochastic event-based modelling approach

Morris Oleng^{1,2,3} · Zuhail Ozdemir¹ · Kypros Pilakoutas¹

Received: 3 February 2023 / Accepted: 30 December 2023
© The Author(s) 2024

Abstract

Uganda lies between the eastern and western arms of the East African Rift System, the largest seismically active rift above sea level. With increasing population, urbanisation and rapid construction, seismic risk in the country is escalating fast and is compounded by the high vulnerability of the building stock and inadequate disaster prevention and mitigation strategies. Hence, there is an urgent need to assess Uganda's resilience against seismic risks. This paper presents a Monte-Carlo based probabilistic seismic hazard model for Uganda, as the first step towards the development of a seismic risk and resilience assessment framework for the country. In addition to fault segment data, earthquake catalogues are compiled for the period between 1900 and 2022 to estimate recurrence parameters for source zones in the area of interest. Area source zones incorporating focal mechanisms are used to stochastically model a national hazard framework for Uganda. A logic tree approach is applied to implement four ground motion prediction equations for both stable continental and active shallow crust geologies. Mean hazard curves, uniform hazard spectra, earthquake disaggregation and spectral pseudo-accelerations for major Ugandan cities are derived in addition to hazard maps for the country. The findings are largely consistent with previous regional studies and confirm that western Uganda is exposed to the highest level of seismicity. The model presented herein can be used to kick-start the update and continuous improvement of Uganda Seismic Design Code and the National Policy for Disaster Preparedness and Management.

Keywords Probabilistic seismic hazard analysis (PSHA) · Monte-Carlo (MC) simulations · Fault-oriented model · Spatially smoothed seismicity · Logic-tree implementation · Uganda

✉ Morris Oleng
wotamuko@gmail.com

Zuhail Ozdemir
z.ozdemir@sheffield.ac.uk

Kypros Pilakoutas
k.pilakoutas@sheffield.ac.uk

¹ Department of Civil and Structural Engineering, The University of Sheffield, Sheffield, UK

² Department of Civil and Environmental Engineering, Kyambogo University, Kampala, Uganda

³ Department of Engineering and Environment, Uganda Christian University, Mukono, Uganda

1 Introduction

The impact of earthquakes on the socio-economic growth and development of communities, particularly in developing countries, can be devastating due to the potentially huge economic and human losses that may result by damage to the natural and built environment. Health, education, infrastructure, economy, politics and institutional governance are amongst the main socio-economic sectors that can suffer consequentially. Over the past decades, several destructive earthquakes occurred in various parts of Uganda; resulting in loss of lives, injuries, physiological distress and damage to property. The recent 2016 Bukoba earthquake left many Ugandans homeless and resulted in high economic losses (USGS 2016), due primarily to the substandard building stock. The proliferation of substandard constructions coupled with rapid population increase and urbanisation exposes Uganda to a massively increasing risk resulting from earthquakes. Hence, there is an urgent need to quantify this risk so that the appropriate mitigation measures can be taken.

Destructive earthquakes in East Africa are largely driven by the East African Rift System (EARS), which is a well-known tectonic feature in the region (Midzi et al. 1999). Due to Uganda's geographical location between the eastern and western arms of the EARS (shown in Fig. 1a), the country has experienced a couple of earthquakes with moment magnitude (M_w) between 6.0 and 7.2. Moreover, many seismic events with $M_w < 6.0$ have been recorded across the country. Despite the existence of the EARS which is largely responsible for earthquakes in the region, little documented evidence of historical events can be found; partly due to historically low population density and poor historical records.

Uganda and the surrounding regions have previously been hit by many catastrophic earthquakes. The location of the EARS relative to major cities and epicentres of the worst events are shown in Fig. 1b. In the past century, the 1929 Masaka earthquake with a body-wave magnitude (m_b) of 5.9 was widely felt across Uganda and was preceded by numerous foreshocks and followed by several aftershocks. In the epicentral region,

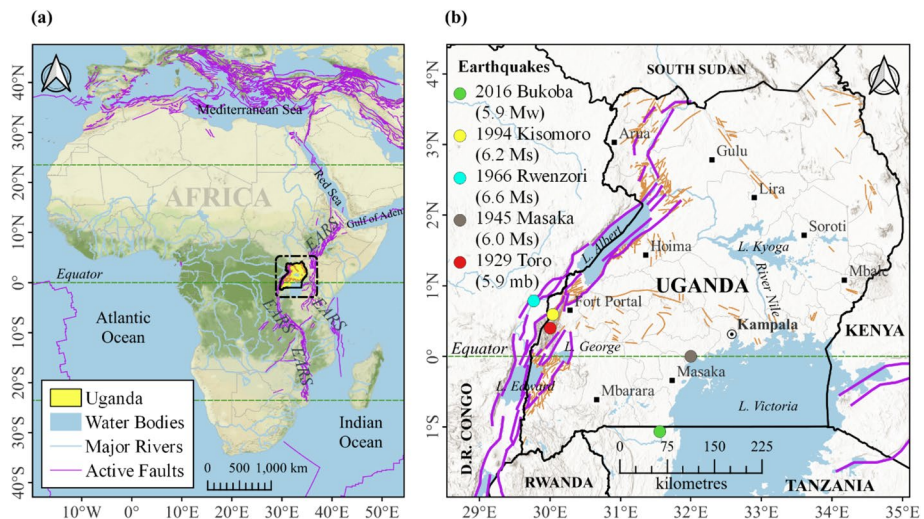


Fig. 1 a Geographical location of Uganda on the African continent, and; b Location of the active fault system (EARS) relative to major cities and epicentral locations of the most destructive earthquakes which occurred in Uganda and around its neighbouring countries

landslides occurred extensively and changes were observed in hot springs (Maasha 1975). In 1945, another earthquake with a surface-wave magnitude (M_s) of 6.0 hit Masaka and caused 5 deaths, several injuries and many building collapses (Bisset 1945; Loupekine 1966; Maasha 1975). The worst event of the twentieth century was an earthquake of 6.6 M_s which struck the Rwenzori region (western Uganda) in 1966; causing 160 deaths, 1300 injuries, and destroying over 7000 houses (Maasha 1975; Sykes 1967). Later in 1994, the Kisomoro earthquake of 6.2 M_s hit the districts of Bundibugyo, Kabarole and Kasese and prompted the emergence of hot springs in Buranga (Sempaya) geothermal field (Cheriberi and Yee 2022; Hampton 1995; Midzi and Manzunzu 2014). The National Earthquake Disaster Committee reported that this event killed 8 people, caused several injuries (NEDC 1994) and economic losses worth US\$ 60 million were incurred in the districts of western Uganda (Kahuma et al. 2006). Recent earthquake events have caused higher economic losses in the region. For instance the 2016 Bukoba earthquake with 5.9 M_w struck north Tanzania on the western shore of Lake Victoria; causing 11 deaths, more than 440 injuries and economic losses estimated in excess of US\$ 458 million in the Kagera region of Tanzania. Although the majority of the effects were felt in the neighbouring country, Rakai district of Uganda (located at the Uganda-Tanzania border) registered 4 deaths and over 590 people were affected in this unprecedented disaster (Balikuddembe and Sinclair 2018).

Even though past earthquakes have resulted in relatively small losses, it is worth noting that damages are likely to escalate due to fast population growth and urbanisation. According to the most recent national census, the population of Uganda increased from 9.5 million in 1969 to 34.6 million in 2014, with a 3% average yearly growth rate between 2002 and 2014. By June 2022, Uganda's population was estimated at over 44.2 million (UBoS 2022). Increased losses may arise due to a growing population of substandard building stock (Hashemi 2017; Twesigomwe 1997). Despite damages due to past earthquakes, seismic design principles are often ignored and as such, the displacement capacity of most existing buildings is not enhanced. Moreover since modern constructions are larger and heavier than traditional constructions, they are inherently more vulnerable to damage in the event of ground motion, especially when seismic design is neglected (Brzev et al. 2013; Vicente et al. 2011).

To manage earthquake risks and significantly reduce fatalities, casualties and economic losses, appropriate pre- and post-disaster risk mitigation strategies ought to be developed and adequately implemented. Whilst several earthquake risk assessment tools such as HAZUS (FEMA 2003) and RADIUS (Villacís 1999) have been developed to manage the associated seismic risks, their applicability in developing countries like Uganda is still difficult; partly due to scarce records of historical earthquakes, lack of empirical data required to calibrate and numerically verify site-response models, and scanty information on active fault characteristics (Sianko et al. 2020). Despite Uganda's lack of detailed information relating to earthquakes, there is high demand for a seismic risk assessment tool which relies on data that can be readily obtained from local agencies or by local surveys.

At a national level, mitigation of earthquake risk largely requires the formulation and implementation of appropriate seismic design codes. The current seismic design guidelines of Uganda (US 319:2003) (UNBS 2003) are not only obsolete, but also not in line with modern seismic design codes like Eurocode 8-1 (CEN 2004). In that respect, there is an urgent need to review and update US 319:2003 (UNBS 2003) so as to reflect advanced understanding of the seismic behaviour of structures developed in recent decades. However, the hazard and socio-economic (including the national building inventory) level of the country need to be quantified first.

Even though future earthquake occurrences cannot be predicted accurately, sufficient understanding of global and local seismology, geology and tectonics is often used to arrive at reasonable estimates of earthquake hazards. This work presents a rigorous probabilistic seismic hazard assessment (PSHA) that relies mostly on the readily available seismic data for Uganda. Using *OpenQuake* engine (Pagani et al. 2014), a stochastic event-based modelling approach is used to generate synthetic earthquake catalogues by randomising key hazard parameters such as epicentral location, maximum magnitude, hypocentral depth, and basic geo-tectonic setting.

This paper commences with a review of previous hazard studies in the region, followed by a sequential description of the underlying methodology adopted. The following sections explain the data collection and processing, seismic source characterisation, and implementation of ground motion prediction equations (GMPEs) used to characterise site response. The remaining parts present and discuss the Monte-Carlo (MC) based PSHA results for Uganda, developed using a fault-oriented spatially smoothed seismicity technique (Pagani et al. 2023; Weatherill 2014).

2 A review of previous seismic hazard studies within and around Uganda

Prompted by the increasing human and economic losses due to previous earthquakes in Sub-Saharan Africa (SSA), several seismic hazard studies have been conducted for Uganda and its neighbouring countries. Twesigomwe (1997) compiled instrumental catalogues from 1900 to 1991 and produced a classical PSHA for Uganda. Earthquake magnitudes were homogenized to M_s scale based on conversion equations suggested by Ericsson (1971). Due to insufficient strong ground motion records, the ground motion prediction relationship of Krinitzsky et al. (1988) was semi-theoretically calibrated. Seismic hazard across Uganda was subsequently described in terms of mean peak ground acceleration (PGA) only. Results show that for a 10% probability of exceedance (POE) in 50 years, western Uganda can expect a PGA of 0.22 g; whereas PGAs between 0.05 and 0.06 g were predicted across the other parts of the country.

Midzi et al. (1999) used the earthquake records compiled by Turyomurugyendo (1996) and *FRISK88M* (McGuire 1996) software to perform a conventional PSHA for Southern and Eastern Africa. Assuming a *Poisson* model of earthquake occurrences, dependent events were removed using the Lazarov and Christoskov (1981) declustering algorithm. Then, the regional GMPEs established by Jonathan (1996) and Twesigomwe (1997) were used to generate hazard maps for a 10% POE in 50 and 100 years. The results show a relatively higher seismic hazard with a maximum PGA raising to 0.27 g along the western arm of the EARS. In another study, Mavonga and Durrheim (2009) used the regional GMPEs of Mavonga (2007b), Atkinson and Boore (2006) and Jonathan (1996) to conduct a classical PSHA for Democratic Republic of the Congo (DRC). A linear regression curve fitting method was used to calculate the Gutenberg-Richter recurrence parameters from the incremental and cumulative values obtained using *Seisan* (Havskov and Ottemöller 2003) software. However, a maximum likelihood method which implicitly makes assumptions regarding the stationarity of events for all periods would give more efficient and unbiased results (Felzer 2008). Nonetheless, the study predicted that Lake Tanganyika rift was prone to the highest level of seismic hazard, in which a maximum PGA of 0.16 g was expected for a 10% POE in 50 years.

Delvaux et al. (2017) performed a classical PSHA based on a novel seismo-tectonic zonation which integrates neotectonic fault systems, seismology, geology, location of thermal springs and basin architecture of the Kivu rift region. One major drawback in this study is that completeness magnitudes were estimated visually from the change in slope of Frequency-Magnitude-Distribution (FMD), yet other statistical approaches appraised by Woessner and Wiemer (2005) would effectively give more realistic estimates. Nevertheless, hazard maps were computed using *R-CRISIS* (Ordaz and Salgado-Gálvez 2017) software and the results indicated lateral variation in tectonic setting and higher PGAs raising to 0.43 g around Bukavu city in eastern DRC. The higher PGAs can be attributed to the use of GMPEs (Mavonga 2007a; Jonathan 1996 and Twesigomwe 1997) that are semi-empirically derived and not calibrated against actual strong motion records.

Another study on the seismicity of the Albertine region used the GMPE suggested by Pankow and Pechmann (2006) and predicted maximum PGA values of 0.256 g, 0.195 g and 0.162 g for 2, 5 and 10% POE in 50 years respectively (Bwambale et al. 2015). As this study focused on the Albertine graben only, outputs cannot arguably be used to assess seismic risk for Uganda, as a whole. Conversely, Cheriberi and Yee (2022) conducted a preliminary PSHA for the entire country. Unfortunately, hazard maps showing 10% POE in 5, 10, 20, 50, 100 and 500 years were produced in terms of PGA only and damped Response Spectral Acceleration (RSA) was not considered in the analysis. In a more comprehensive pilot study by the Global Earthquake Model (GEM) and *AfricaArray*, Hazard Modeller's Toolkit (HMTK) (Weatherill 2014) was used to explicitly perform an assessment of seismic hazard related to the EARS (Poggi et al. 2017). Even though this study investigated the entire SSA with a fairly wide mesh of 10 km, the results were largely consistent with the previous Global Seismic Hazard Assessment Project (GSHAP) model initially proposed by Midzi et al. (1999).

This study presents a detailed compilation and refinement of the Uganda earthquake catalogue, prior to the estimation of the associated recurrence parameters. Herein, the zonation proposed incorporates the geology and seismo-tectonic setting of the country in a more refined manner; with the investigation area comprising a mesh spacing of 2.5 km. Although site-dependent hazard predictions may be useful, additional bedrock hazard results are derived by assuming free rock conditions with a fixed 30 m average shear-wave velocity reference of 760 m/s assigned to each site of the investigation mesh. Whereas past studies have largely utilised the conventional PSHA method, the novelty of this work is that it employs a MC-based PSHA approach. Herein, physics-based GMPEs are implemented to generate ground motion fields from which intensity measures are simulated at various locations in Uganda. The MC-based PSHA model developed in this study can be used to propose more realistic elastic and design response spectra for a new version of the Uganda seismic design code, towards enhancing the country's resilience against future earthquake risks.

3 Geology, tectonics and morphology of Uganda

The tectonic history of Africa is largely characterised by the EARS, a divergent continental plate boundary superimposed on the African plate (Chorowicz 2005; Ebinger 1989). The EARS is an extension plate boundary between the Nubian and Somalian plates, opening at an average annual rate of 6–7 mm (Fernandes et al. 2004). With time, as the Nubian and Somalian plates move further away from each other, the area between

them will drop below sea level as the crust grows thinner. This phenomenon could eventually lead to the formation of a new oceanic lithosphere along the centre of the rift, thus producing a new narrow ocean basin with its own mid oceanic ridge (Chen and Scawthorn 2003; Macgregor 2015).

The orientation of the rifts, highlands and associated volcanic activity suggests that rifting of the continental lithosphere (36–43 km thickness) is possibly due to a rising mantle plume formed beneath the *Afar* region. Accompanied by large flood basalts, this rifting causes stretching and fracturing of the brittle lithosphere (Kampunzu et al. 1986). Since Uganda is located between the two active arms of the EARS, its unique geography and morphology offer an ideal basis for observing the seismicity, tectonics and geological processes associated with the rift system. A review of Uganda’s geology and geodynamic development from historical data indicates that extensive variations in geochronological, structural, petrologic and geochemical development have been recorded during a long geological timescale of over three billion years (Maasha 1975; Schlüter 2008). As presented in Fig. 2, Uganda’s geology largely comprises Neo and Mesoarchean lithospheric fragments welded together by Palaeo, Meso and Neoproterozoic fold belts. A few regions consist of Neogene, Paleogene and Permian-Upper Carboniferous segments of Phanerozoic structure (Westerhof et al. 2014). In light of Uganda’s geology and seismo-tectonic environment, the major features responsible for the seismicity of the country are shown in Fig. 2; and these include:

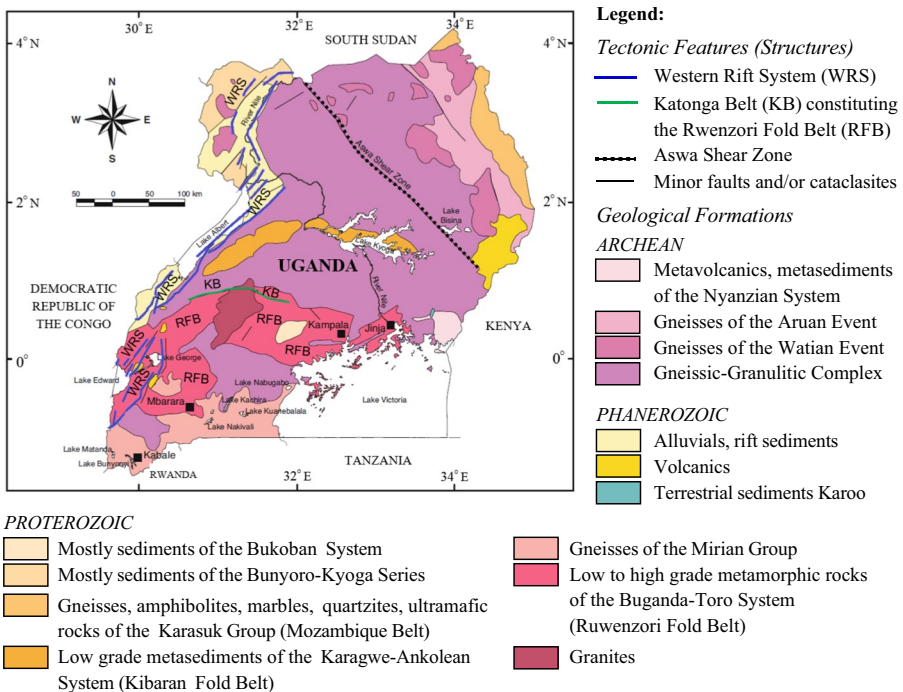


Fig. 2 Map of Uganda showing the generalised geology and major tectonic features responsible for the seismicity of the country (MacDonald 1966; Muwanga et al. 2001; Schlüter 2008)

1. The EARS is an approximately 4000 km long Cenozoic age continental rift stretching from *Afar* triple junction to western Mozambique. Its geology mainly consists Precambrian metamorphic rocks, sedimentary rocks of Miocene age, and a series of Neogene and quaternary lacustrine and fluvial deposits (Fairhead and Stuart 1982; Sykes and Landisman 1964). The development of the EARS, whose magmatically very active eastern branch contains the world's most potassium-rich rocks, is attributed to the Neogene extension (Albaric et al. 2010). The formation of the EARS likely started from Turkana rift located along its eastern branch (Furman et al. 2006; McDougall and Brown 2009); followed by its western arm which has a larger concentration of earthquakes starting from South Sudan and terminating in Malawi (Roberts et al. 2012). It is worth noting that the EARS is amongst the world's most seismically active continental rifts (Asefa and Ayele 2021). Uganda's western border lies along the Western Rift System (WRS) of the EARS. The northern segment of the WRS (Albertine and Rwenzori rifts) is the locus of the Rwenzori Mountains, which is a peninsula of up to 5109 m in altitude and the world's most extreme expression of rift-flank uplift (Maasha 1975; Twesigomwe 1997). The WRS is composed of a series of linked half-graben basins (typically 80–160 km long and 30–60 km wide) which are occupied by large lake systems (Karp et al. 2012).
2. The geology of the Rwenzori Fold Belt (RFB), which stretches from the boughs of the Rwenzori Mountains in western Uganda, mainly comprises Paleoproterozoic low to high grade metamorphic rocks of the Buganda-Toro system and selected sediments of undifferentiated Granites. Geological evidence shows that faulting observed along the RFB continues across Lake Victoria to Speke Gulf and Kavirondo rift in south-western Kenya; and terminates across the Tanzanian border (Darracott 1974; McConnell 1972). These are generally strong tectonic nature folds of east to west orientation; and are superimposed on the Archean rocks of Uganda's shield (Cahen et al. 1966; Spooner et al. 1970; Tanner 1970). Numerous tertiary and quaternary faults strike parallel to the general trend of the RFB; partly due to the initially imposed uplift stresses in western and eastern Uganda, and down warping of the Lake Victoria basin (Maasha 1975).
3. Other than the WRS and RFB which have over time experienced low and moderate seismicity, the other parts of the country constituting the Uganda craton have (in the past) recorded little seismicity. The major tectonic feature in this shield is the *Aswa* Shear Zone, which is a cataclasis superimposed on a stable continental crust (Gneissic-Granulitic Complex) (Schlüter 2008). Therefore, the *Aswa* Shear Zone typically exhibits inactive seismicity except at its northern end where it intercepts the WRS (Hartnady et al. 1992).

On the other hand, Uganda has previously experienced some volcanic activity, for instance across the Elgon and Muhabura mountains, in addition to fault-related seismicity. Recently, the National Geophysical Data Center in conjunction with the World Data Service reported catastrophic impacts due to the May 2021 volcanic eruption of Mountain Nyiragongo, located 10 km from Goma in the neighbouring DRC (NGDC and WDS 2022). Although volcanic activity is not included in this work, future studies will aim at the development of the associated volcanism hazard assessment framework for Uganda.

4 Monte Carlo (MC) based PSHA: methodology

In this work, the stochastic event-based PSHA calculator for distributed seismicity, embedded within the *OpenQuake* engine (Pagani et al. 2014), is used to perform a MC-based PSHA which relies on earthquake data available for Uganda. Regarding source typologies, the present study adopts area source zones (ASZs) which are tectonically and seismically homogeneous. ASZs are treated independently, and the *Poisson* model is assumed for all possible rupture scenarios (Crowley 2005; Johnson and Pagani 2021). For each rupture scenario, sample realisations from each intensity measure are determined using MC simulations (Musson 1999).

The MC-based procedure for predicting seismic hazard at a particular site of interest essentially starts with earthquake catalogue refinement through magnitude harmonisation, declustering and completeness analysis; prior to delineating ASZs based on geological, seismological and spatial distribution of earthquakes. Following the procedure proposed by Crowley and Bommer (2006), synthetic earthquake catalogues (occurrence, magnitude and location of event in a particular year) are then produced by randomizing key parameters obtained from past seismicity, tectonic regimes and geological data to represent the future seismic behaviour of the area of interest. The distances between earthquake events (from all sources) and the sites of interest are then computed for each year of synthetic catalogue. The ground motion intensities at a particular site are calculated using GMPEs, fault typologies and soil parameters. The ground shaking intensities at a specific site due to all events occurring in a particular year of synthetic catalogue are then determined. This process is repeated for a given number of simulations; for instance 1000 simulations of 100 years of earthquake catalogue. All ground motion levels at a given site are subsequently combined and sorted in decreasing order of severity. Finally, ground shaking values at a specific site for the desired return periods are determined; and the process repeated for all sites (Sianko et al. 2020).

As opposed to the conventional PSHA method, the MC-based PSHA approach provides several advantages because of its convenience when applying physics-based GMPEs in which intensity measures are computed as realisations instead of probability distributions (Graves et al. 2011). This stochastic modelling approach is beneficial for spatially distributed seismicity where intensity measures are simulated at various locations, thereby allowing model flexibility. On the contrary, the computational cost of the MC-based PSHA is quite demanding as such simulations produce a substantial amount of data. Moreover, a sufficient number of realisations ought to be simulated to generate an adequate number of stochastic event sets (Baker et al. 2021). Additional descriptions of a stochastic event-based PSHA using MC simulations can be found in literature (e.g., McGuire 2004; Field et al. 2003 and Musson 1999).

5 Earthquake catalogue for Uganda

In PSHA, earthquake catalogues are required to quantify seismicity, determine seismic source zonation and parameters associated with earthquake occurrence in such source zones, and to generate synthetic earthquake catalogues. The first step taken towards performing a PSHA is to compile and merge existing historical and instrumental catalogues prior to homogenisation, declustering and completeness analyses. Considering the design

earthquake for SSA, a minimum buffer zone of at least 50 km is assumed within the selected geographical area (-2.7° to 5.9° North, 28.1° to 36.5° East) for acquisition of earthquake data. The GEM catalogue toolkit (Weatherill et al. 2016) is then used to update the earthquake records. The following sections describe the steps taken to produce and refine the earthquake catalogue for Uganda.

5.1 Catalogue compilation

The first earthquake catalogue is obtained locally from the Directorate of Geological Survey and Mines (DGSM), under the Ministry of Energy and Mineral Development (MEMD) in Uganda. However, due to the existence of large solution uncertainties caused by insufficient station coverage and absence of historical records, catalogues are obtained from other credible global agencies and bulletins. Then, earthquake catalogues from global databases are merged with the records from DGSM. Considering all events with $M_w \geq 4$ as the minimum threshold capable of causing structural damage, all catalogues are selected and prioritised as follows:

5.1.1 ISC-GEM catalogue

This global instrumental catalogue, compiled by International Seismological Centre (ISC) in conjunction with GEM, is a refined version of the ISC bulletin (ISC 2022) and with all event magnitudes homogenised to the M_w scale. It presents an improvement on the accuracy of the location and magnitude for events with $M_w > 5.5$, and occurring between 1900 and 2014 (Di Giacomo et al. 2018; Storchak et al. 2013, 2015). In this work, 84 events are recorded in the ISC-GEM catalogue. This catalogue is prioritised over the other global bulletins because it is refined. Since the ISC-GEM catalogue includes hypocentral depths for all events, its records are primarily adopted to perform reasonable statistical analyses of hypocentral depth distribution across the study area.

5.1.2 USGS catalogue

This is a global database consisting of seismic data recorded by the United States Geological Survey (USGS 2022). Although event magnitudes are later harmonised to the M_w scale, events in this database are recorded using various magnitude scales. For the study region, this database recorded 364 events (out of 1512 events), including the hypocentral depths of all events. In this work, the records obtained from the USGS catalogue are given second priority.

5.1.3 ISC reviewed bulletin

This bulletin initially provided one of the primary earthquake catalogues which are manually reviewed by ISC, with a coverage which dates to the start of the twentieth century (ISC 2022). In this bulletin, event magnitude scales vary between time periods and agencies. For the selected geographical area, it contains 671 events (out of 1512 compiled events) spanning between 1903 and 2022. However, hypocentral depths of some events are not recorded. In that respect, events recorded in the ISC bulletin are prioritised after the USGS catalogue.

5.1.4 DGSM catalogue

The DGSM, an agency under MEMD, is mandated with the responsibility of monitoring and recording earthquakes in Uganda. Earthquake datasets obtained are recorded in the M_s scale and span from 1970 to 2022. A total of 842 events are recorded within and around Uganda. However, these include small-magnitude ($M_s < 4.0$) events that are ignored in subsequent analyses. Thus, only 250 events with $M_s \geq 4.0$ are considered. The hypocentral depths of all events are recorded in this catalogue (DGSM 2022). The agency recommended ISC reviewed bulletin (ISC 2022) as a reliable record for events that occurred before 1970. Accordingly, the DGSM catalogue is given fourth priority during duplicate identification and removal.

5.1.5 GEM global historical earthquake archive

This archive is a collection of reviewed global historical events, which generally comprises of 825 large magnitude earthquakes that occurred between 1000 and 1903 (Albini et al. 2013). Due to the plausible lack of historical records in SSA, additional events are obtained from the reappraisal of major African earthquakes between 1900 and 1930 (Ambraseys and Adams 1991). In total, both of these compilations contained only 2 events within Uganda and around its immediate environs. In the process of merging the catalogue for Uganda, all events compiled from the GEM global historical earthquake archive are used directly without prioritisation.

5.1.6 Compilations from literature

A summary of previous earthquakes in Uganda and its vicinity between 1912 and 1973 was compiled from published studies (e.g., Fairhead and Girdler 1971; Fairhead and Stuart 1982; Gutenberg and Richter 1941; Rothé 1969 and Sutton and Berg 1958). Out of the 1512 events, 134 are obtained from this compilation (Maasha 1975). Although earthquake magnitudes were harmonised to the m_b scale, the depths of some events were unfortunately not recorded. Hence, this dataset is least prioritised when generating the final earthquake catalogue for Uganda.

5.2 Duplicate finding and catalogue merging

Since the Uganda earthquake catalogue used in this work is compiled from several databases, it is important to identify and remove duplicate events before the catalogue refinement process. This is because different bulletins have their own versions of the origin time, location, accuracy of measurement, and magnitude scales etc. After merging catalogues from different sources, earthquakes falling within a prescribed temporal and spatial window are assumed to represent the same seismic event. Different studies have attempted to define time and space windows for duplicate removal. For instance Jones et al. (2000) proposed that two events may be considered duplicates if they differ by less than 100 km and 16 s in space and time respectively. However, Jónasson et al. (2021) discovered that the suggested window was too strict and rather proposed 320 km

and 16 s. The most appropriate window should be decided based on the seismic network, geology and seismo-tectonics of the region in question.

In this regard, a more representative pilot study by GEM and *AfricaArray* (Poggi et al. 2017) indicated relative uncertainties between agencies recording and reporting events in SSA. The study noted that larger windows gave erroneous results by misrepresenting earthquakes in an aftershock sequence as duplicates. Accordingly, best results were obtained with a space and time windows of 0.5° (approximately 55.5 km) and 120 s respectively. Since Uganda lies within SSA, it is likely that the country’s geology and seismo-tectonics are similar. Therefore, this study adopts the same windows to identify and remove duplicate events. Employing these windows gives 768 duplicate events (out of 1512). The final updated earthquake catalogue consists of 744 major events (excluding duplicates and before declustering) that occurred in Uganda and its surroundings, starting from the twentieth century.

5.3 Homogenisation

Following catalogue merging and removal of duplicate seismic events, the magnitude of events is harmonised to the M_w scale. Due to lack of calibration data for Uganda, this study prioritises more credible globally proposed magnitude conversion equations. A summary of the list of agencies and their respective conversion equations, largely adopted from Poggi et al. (2017), is presented in Table 1.

Figure 3a shows the distribution of seismicity over time for all events in the merged, homogenised, but non-declustered earthquake catalogue for Uganda. Event distribution is not uniform over the investigated period as there are more events reported after 1957, especially for lower magnitudes. This can be attributed to the contribution from seismic monitoring stations like the Lwiro network established in the 1950s. According to DGSM (2022), the installation of several seismic networks (e.g., Entebbe station in 1991, Hoima and Kilembe in 1992, Dundu in 1995, and Kyahi station in 1999) is partly responsible for

Table 1 Agencies and their corresponding moment magnitude conversion equations

Agency	M_w conversion rule	Range	References
ISC	$0.616 M_S + 2.369$	$M_S < 6.0$	Weatherill et al. (2016)
	$0.994 M_S + 0.1$	$M_S \geq 6.0$	
	$1.084 m_b - 0.142$	$m_b < 6.5$	
NEIC	$0.723 M_S + 1.798$	$M_S < 6.5$	
	$1.005 M_S - 0.026$	$M_S \geq 6.5$	
	$1.159 m_b - 0.659$	$m_b < 6.5$	
PRE	M_L	$M_L < 6.0$	Assumed 1:1 scaling and arbitrary uncertainty (0.3)
BUL	M_{b1g}	$M_{b1g} < 6.0$	
TZB, ETP, AAE	$1.02 + 0.47 M_L + 0.05 M_L^2$	$M_L < 5.0$	Edwards et al. (2010)
PAS	$0.616(M_S - 0.2) + 2.369$	$M_S > 6.0$	ISC- M_s corrected, as suggested in Engdahl and Villaseñor (2002)
	$0.994(M_S - 0.2) + 0.1$	$M_S < 6.0$	

Acronyms defining the agencies are taken from the ISC website (Contributing agencies (isc.ac.uk), accessed on 21 June 2022). For prioritization, agencies are sorted in decreasing order

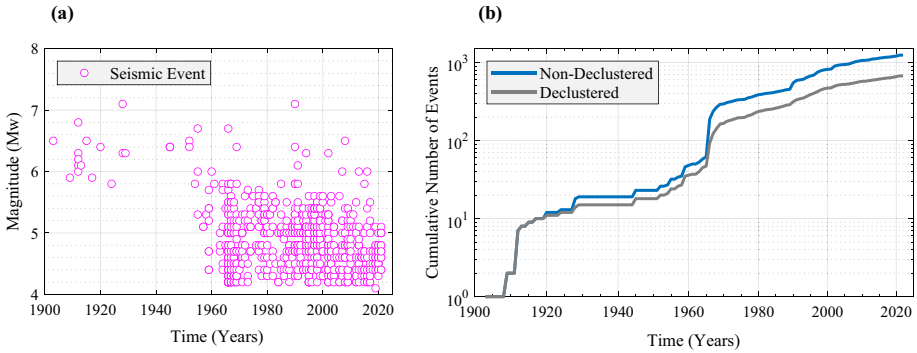


Fig. 3 **a** Distribution of seismicity over time for the events in the homogenised, non-declustered earthquake catalogue for Uganda; and **b** Comparison between cumulative distribution of earthquakes before and after fore-/aftershock cluster removal

the recent increase in reporting of earthquakes (especially small magnitude events) within and around Uganda.

5.4 Declustering

The sequence of earthquakes often features numerous aftershocks and foreshocks which are related to the mainshocks. In as much as these correlated events are not necessarily irrelevant in seismic hazard and risk assessments (Boyd 2012), it is vital to decluster seismicity data through a systematic identification of earthquake clusters before estimating mean occurrence rates. Several algorithms (e.g., Gardner and Knopoff 1974; Reasenber 1985; Knopoff 2000 and Bustos 2009) have been developed to apply fixed distance and time windows for finding correlated events using magnitude bins of each mainshock. The HMTK (Weatherill 2014) is used to run the original Gardner and Knopoff (1974) algorithm; together with the subsequent modifications by Grünthal (van Stiphout et al. 2012) and Uhrhammer (1986) described in Eqs. (1), (2) and (3) respectively.

$$d = 10^{0.1238M+0.983} \quad t = \begin{cases} 10^{0.032M+2.7389} & \text{if } M \geq 6.5 \\ 10^{0.5409M-0.547} & \text{else} \end{cases} \quad (1)$$

$$d = e^{1.77+(0.037+1.02M)^2} \quad t = \begin{cases} e^{-3.95+(0.62+17.32M)^2} & \text{if } M \geq 6.5 \\ 10^{2.8+0.024M} & \text{else} \end{cases} \quad (2)$$

$$d = e^{-1.024+0.804M} \quad t = e^{-2.87+1.235M} \quad (3)$$

where *d* is the distance window (in km), *t* is the time window (in days), and *M* is the earthquake size (preferably in the moment magnitude scale)

For each assumed earthquake mainshock, fixed distance and time windows required to isolate and remove correlated/clustered events from the sorted catalogue are calculated using Eqs. (1–3). Additionally, the Knopoff (2000) procedure provides window parameters for events ranging in magnitude between 4.2 and 6.0. Following tendencies of time and distance windows from Gardner and Knopoff (1974), Bustos (2009) modified the Knopoff (2000) procedure by extrapolating the spatial and temporal windows for events with

magnitude greater than 6.0. Subsequently, a code (MATLAB 2021b) is developed to run the modified Knopoff (2000) algorithm extended by Bustos (2009).

The number of mainshocks and dependent events in the refined catalogue according to each algorithm is listed in Table 2. For instance, the declustered catalogue consists of 543 events out of the original 744 (approximately 27% removal of dependent events) in the range of $4.1 \leq M_w \leq 7.2$ following the modified Knopoff (2000) algorithm. The results show that other declustering algorithms remove more events due to larger windows. Therefore, as a conservative approach for estimating seismicity rates of occurrence, the declustered catalogue based on modified Knopoff (2000) algorithm is adopted in subsequent analyses.

A comparison between cumulative distribution of earthquakes before and after removal of dependent events for all $M_w \geq 4$ events that occurred between 1903 and 2022 is shown in Fig. 3b. The plot shows that the number of events in the declustered catalogue is less than those in the non-declustered data by approximately 27%. This plot is similar to the analysis done by Poggi et al. (2017); although more earthquake events were removed in their work since the original Gardner and Knopoff (1974) declustering algorithm was employed, notwithstanding the much wider area comprising many more earthquake records.

5.5 Completeness analyses

Earthquake catalogue completeness procedures (e.g., Alamilla et al. 2015; Hafiez 2015 and Stepp 1972) characteristically involve identifying magnitude thresholds for which significant departures from the expected occurrence rates are observed. For each magnitude level, the catalogue completeness periods may start at different points in time. Whilst large magnitude events are often complete from earlier dates in time, small magnitude earthquakes tend to be complete for recent periods (Sianko et al. 2020). In undertaking completeness analysis for the Uganda catalogue, Stepp (1972) procedure is first implemented using the HMTK (Weatherill 2014). However, this algorithm gives erroneous results for large magnitudes, possibly because of sparse and largely irregular data coverage. Subsequently, completeness magnitude (M_c) values are determined statistically using maximum curvature (Wiemer and Wyss 2000) and *b-value* stability (Cao and Gao 2002) methods; in combination with a bootstrapping mechanism (Michael 1987) to cater for uncertainties. Although the use of day-to-night ratio of earthquake frequency method suggested by Rydelek and Sacks (1989) could have been a suitable alternative, previous studies (e.g., Di Giacomo et al. 2015) employed non-parametric and straightforward techniques like the maximum curvature method of Wiemer and Wyss (2000) which gives statistically robust estimates of the M_c values (Mignan and Woessner 2012).

Table 2 Summary of non-Poissonian events removed using various algorithms

Algorithm	Mainshocks	Events removed	Percentage of events removed (%)	Clusters removed (%)
Gardner and Knopoff (1974)	365	379	50.54	101
van Stiphout et al. (2012)	309	435	58.13	98
Uhrhammer (1986)	511	233	30.76	70
Musson (1999)	485	259	34.28	76
Modified Knopoff (2000)	543	201	27.02	99

The Uganda catalogue is eventually divided into six periods (1900–1929, 1930–1959, 1960–1964, 1965–1969, 1970–1979, and 1980–2022) after subsequent adjustments based on network coverage and station spacing. Next, the ZMAP (2022) code of Wiemer (2001) is used to evaluate completeness thresholds and results plotted as shown in Fig. 4. While the red lines indicate completeness magnitudes and periods, the yellow shaded area marks the incomplete dataset which is excluded from further analysis. Although deciding the completeness period for different magnitudes can be very subjective, it is concluded herein that the Uganda catalogue is complete for: $M_w \geq 4.5$ from 1980, $M_w \geq 4.8$ from 1970, $M_w \geq 4.9$ from 1965, $M_w \geq 5.3$ from 1960, $M_w \geq 5.6$ from 1930 and $M_w \geq 6.0$ from 1900. The completeness thresholds are in good agreement with the fact that for higher magnitudes, the completeness periods start from earlier dates while smaller magnitude events are often complete for recent time periods.

6 Seismic source characterisation

Seismic source characterisation involves identifying and defining all possible rupture scenarios that could produce ground shaking within the model coverage area. Using fault characteristics, observed seismicity and geo-tectonic setting, a rupture scenario is mainly characterised by earthquake magnitudes and their epicentral locations, in addition to its likelihood of occurrence (Bommer 2022). This section discusses the steps taken to characterise earthquake sources within and around Uganda.

6.1 Zonation

Whilst there are many legitimate zonation modelling approaches, a typical strategy involves preparing the earthquake catalogue, dividing the region of interest into tectonic domains, choosing and defining source geometries and typologies, and assigning activity rates to each source zone (Baker et al. 2021; Vilanova et al. 2014). Herein, a mixed approach that accounts for observed seismicity and geo-tectonic characteristics of Uganda is adopted; principally assuming that each zone has reasonably uniform seismicity and zonation is in harmony with regional geo-tectonics. The methodological framework of this approach involves assessing a suitable scale and degree of

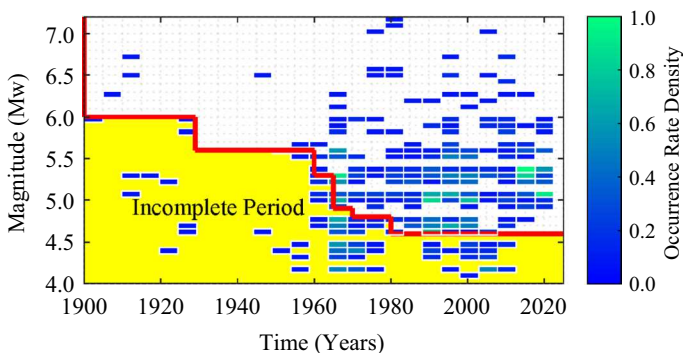


Fig. 4 Magnitude-time-density plot of the Uganda catalogue, with normalised rates computed for a 0.1 magnitude bin and a fixed time window of 5 years

stationarity, completeness thresholds, and credibly ranking physical criteria used to delineate ASZs. The application of this zonation strategy subsequently splits the study area into 13 ASZs. In addition to the fault system and epicentral location of major earthquakes within and around Uganda, the area source zonation model used in the MC-based PSHA is shown in Fig. 5. The fault system shown in Fig. 5 is obtained from the global homogenised database developed by GEM Foundation (Styron and Pagani 2020).

ASZs of similar geology and tectonic settings are subsequently categorised into four gross sources. Zones 1–5 are grouped to constitute the WRS category; zones 9, 10 and 12 are combined to form the RFB category stretching across to Speke Gulf and Nyanza rifts via Lake Victoria basin; the third gross source group consists of zones 8 and 13, representing the Eastern Rift System (ERS) category; and zones 6, 7 and 11 constitute the Congo-Uganda-Tanzania (CUT) craton. This approach is necessary for determining occurrence rates since certain zones recorded very few events which would not give reliable estimates of seismicity parameters.

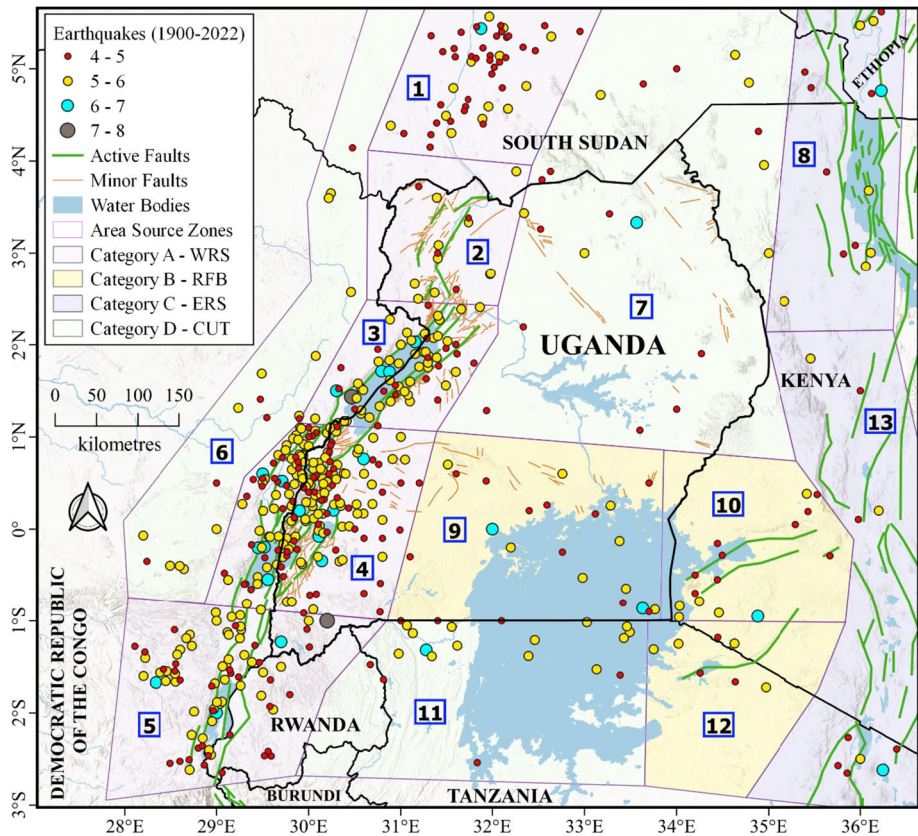


Fig. 5 Earthquake epicentres, active and minor fault systems, and area source zonation model used to perform the MC-based PSHA for Uganda

6.1.1 Category A: western rift system (WRS)

Within the study region, the WRS exhibits the largest rate of earthquake occurrence, although with limited volcanism. The northern part (Zone 2) is characterised by a series of faults which form part of the rift striking in the north–south direction (Ebinger 1989; Twesigomwe 1997). The WRS category includes the Albertine rift and is bounded between the south–southwest and north–northeast Lake Albert basin, east–west trending River Nile, and north–south trending Nile rift. Also, the Rwenzori mountain block is characterised by the Virunga volcanoes linked with a transverse fracture zone along the western rift axis (Kampunzu et al. 1986; Maasha 1975).

The WRS is dominated by relatively strong seismic events which spread throughout the lithosphere and many large magnitude events have occurred within the lower crust, with hypocentral depths between 30 and 40 km (Yang and Chen 2010). For selected fault sections along the WRS, the variation of earthquake hypocentral depths with time is presented in Fig. 6a–d. Along the Albertine rift, the largest events (7.0 M_w and 6.4 M_w) strike deeper in the lithosphere (35 km and 32 km respectively) as shown in Fig. 6a, b. Whereas hypocentral depths of larger earthquake ($M_w > 4.6$) fall within 21 km, events less than 4.6 M_w have occurred beyond 21 km depth along the Rwenzori rift as seen in Fig. 6c, d. This observation is consistent with findings from previous studies (e.g., Brazier et al. 2005; Craig et al. 2011 and Nyblade and Langston 1995). On the other hand, larger hypocentral depth values are computed for more recent earthquakes. This is partly attributed to the recent increase in the number of earthquake recording instruments from which more accurate hypocentral depth solutions are obtained.

The variation of focal depth solutions across a horizontal section through fault lines is plotted for two example cross-sections along the WRS. Whilst Fig. 7a shows depth variation through the Rwenzori rift, a similar variation across the Albertine rift is presented in Fig. 7b. It can be seen that earthquakes with epicentres closer to the faults (green lines) generally occur at greater depths compared with those further from the faults; although a few exceptions are observed. In delineating ASZs falling within the WRS, consideration is given to the observed seismicity, existing focal mechanism and fault orientation data (Macgregor 2015). Therefore, the WRS consists of five ASZs (shown as Zones 1, 2, 3, 4, and 5 in Fig. 5) covering various segments of the western branch of the EARS.

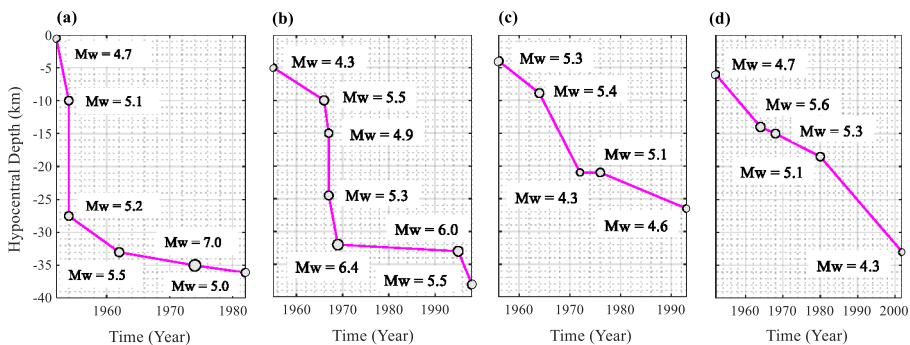


Fig. 6 Cross-sections through specific example faults along the two arms of the western rift system in source category A: **a** Left arm of the Albertine rift; **b** Right arm of the Albertine rift; **c** Left arm of the Rwenzori rift; **d** Right arm of the Rwenzori rift

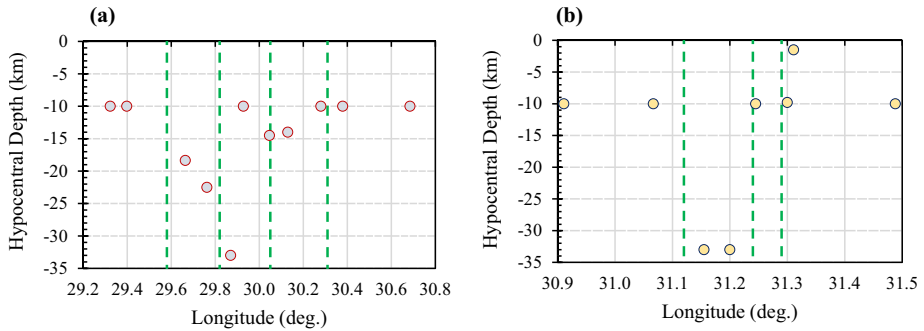


Fig. 7 Variation of hypocentral depths across horizontal cross-sections through selected active faults (*green lines*) in the Western Rift System: **a** Rwenzori rift (Zone 4), and **b** Albertine rift (Zone 3)

6.1.2 Category B: Rwenzori fold belt (RFB)

This category encompasses Nyanza, Speke and Utimbere rifts as well as the connected Katonga faults. It is characterised by Tertiary and Quaternary faults which strike parallel to the Katonga rupture faulting zone; thus, capable of producing earthquakes of moderate intensity (Hartnady et al. 1992). The RFB is dominated by stable zones of seismicity originating from Tanzania and its geo-tectonic environment is largely stable (Furman et al. 2004). Geophysical evidence shows that the lithosphere is 150–200 km below the Precambrian basement and ground shaking levels are possibly lower compared to the surrounding active rift zones (Petit and Ebinger 2000; Saria et al. 2014). This source category contains three ASZs (shown as Zones 9, 10 and 12 in Fig. 5) whose boundaries are predominantly delineated based on seismicity.

6.1.3 Category C: eastern rift system (ERS)

The ERS is bounded by major faults that form the main parts of the eastern arm of EARS and comprises of two source zones, shown as Zones 8 and 13 in Fig. 5, starting from Turkana basin and running southwards along the Victoria microplate. The ERS is characterised by extensive grid faulting, geothermal and volcanic activity (Baker et al. 1972; Chorowicz 2005; Dawson 1992; Yang and Chen 2010). Moreover, Twesigomwe (1997) indicated that the ERS comprises a diffusion fault which links its southern and northern segments. Since the ERS has few records of seismicity, geo-tectonics are mainly considered in its zonation. Further consideration is given to the zone's physical location as it lies between the Ethiopian plateau and Kenyan dome.

6.1.4 Category D: Congo-Uganda-Tanzania (CUT) craton

This source category is intersected by the Precambrian Aswa shear zone, which is largely stable and inactive. The geology of the CUT craton mainly comprises high-grade Metamorphic rocks and Archean granitic green stones. Although the zone mainly exhibits inactive tectonic features, some earthquake events have been recorded especially around Lake

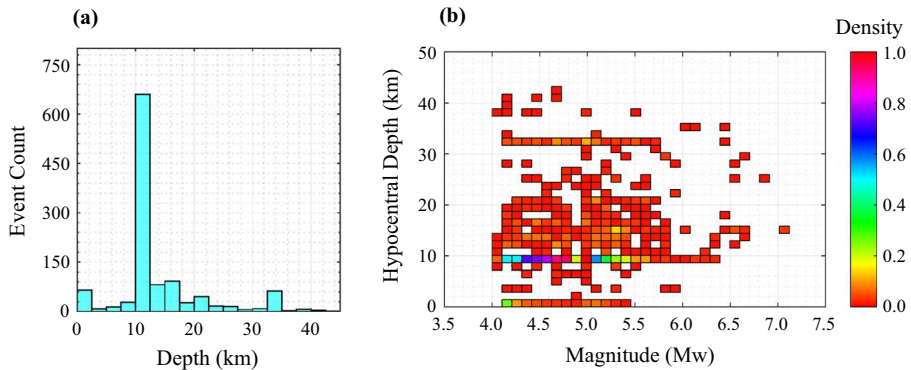


Fig. 8 a Event hypocentral depth count b Magnitude-depth density plot

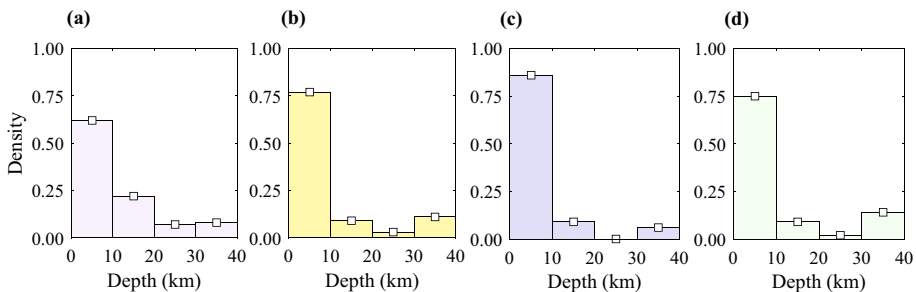


Fig. 9 Distribution of hypocentral depth solutions of earthquakes falling within the four seismic source categories defined in the zonation: **a** Category A (WRS)—442 events, **b** Category B (RFB)—35 events, **c** Category C (ERS)—35 events, and **d** Category D (CUT craton)—56 events

Victoria (Mavonga and Durrheim 2009; Poggi et al. 2017; Twesigomwe 1997). This source category contains three ASZs (shown as Zones 6, 7, and 11 in Fig. 5) whose borders are principally delineated based on geological features and micro-plate boundaries.

6.2 Focal depth distribution

Although hypocentral depths of some events are unknown, a reasonable statistical analysis based on the available samples is considered sufficient. In addition to events whose hypocentral depths have been explicitly assigned a priori, earthquakes of unrecorded focal depth solutions are excluded from this analysis. The hypocentral depth histogram presented in Fig. 8a and magnitude-depth density plot shown in Fig. 8b indicate that most events occur between 10 and 15 km, with very few occurring up to a maximum depth of 45 km. Moreover, larger magnitude events ($M_w > 6.5$) mostly occur at depths greater than 10 km. This is consistent with previous studies (e.g., Rykounov et al. 1972; Shudofsky 1985; Tanaka 1983 and Tongue et al. 1994) which indicate that most earthquakes in East Africa occur at shallow depths of less than 25 km. In addition, the distribution of hypocentral depths of earthquakes falling within the four source categories is shown in Fig. 9a–d.

While many earthquakes are reported at depths raising to 40 km, it can be observed that the largest contribution ranges between the depths of 0 and 10 km across all source

groups. Because of its seismically active nature, it is obvious that seismic source category A (WRS) recorded the highest number of events contributing to focal depth solutions. Notably, the least contribution of event depths falls between 20 and 30 km across all source categories.

6.3 Seismicity analysis

6.3.1 Magnitude-frequency distribution

The seismicity of a region, modelled with parameters (*a*- and *b*-values which are defined within the Gutenberg-Richter recurrence law) reflecting the characteristics of ASZs, describes the relationship between the frequency of occurrence and magnitude of earthquakes (Gutenberg and Richter 1944; Ishimoto 1939). There are several approaches (e.g., Aki 1965; Bender 1983 and Kijko and Smit 2012) which can be used to define the seismicity of a given region.

In this work, earthquake recurrence parameters and their associated standard deviations are estimated using the Weichert (1980) algorithm. This approach is a maximum likelihood method in which different periods of completeness for different magnitude thresholds are considered. Furthermore, the algorithm implicitly makes assumptions regarding stationarity of events for all periods, thereby considered efficient and unbiased for most applications (Felzer 2008). In its subsequent application, Gutenberg-Richter recurrence parameters are firstly determined for the entire catalogue; and then, independently for each seismic source category because of the limited records available, especially for certain ASZs. The *a*-values (shown in Table 3) for each ASZ are estimated by imposing the initially calibrated *b*-values. The plots showing recurrence parameters for the four source categories are presented in Fig. 10a–d.

6.3.2 Maximum magnitudes

Approximation of the maximum magnitude (M_{max}) for use in PSHA is a complicated, and often contentious process that is guided by geology and seismo-tectonic information of the

Table 3 Seismicity parameters for ASZs used in MC-based PSHA for Uganda

Category	ASZ	M_{min}	M_{max}	<i>a</i> -value	<i>b</i> -value	$\sigma(b)$
A. WRS	1	4.0	6.7	3.080	0.96	0.038
	2	4.0	6.4	7.937		
	3	4.0	7.6	3.056		
	4	4.0	7.2	3.645		
	5	4.0	7.7	3.216		
B. RFB	9	4.0	7.0	1.721	0.86	0.139
	10	4.0	7.0	2.276		
	12	4.0	6.1	4.576		
C. ERS	8	4.0	6.7	2.935	0.79	0.215
	13	4.0	7.0	2.107		
D. CUT craton	6	4.0	6.2	1.683	0.67	0.123
	7	4.0	7.0	2.466		
	11	4.0	6.6	1.978		

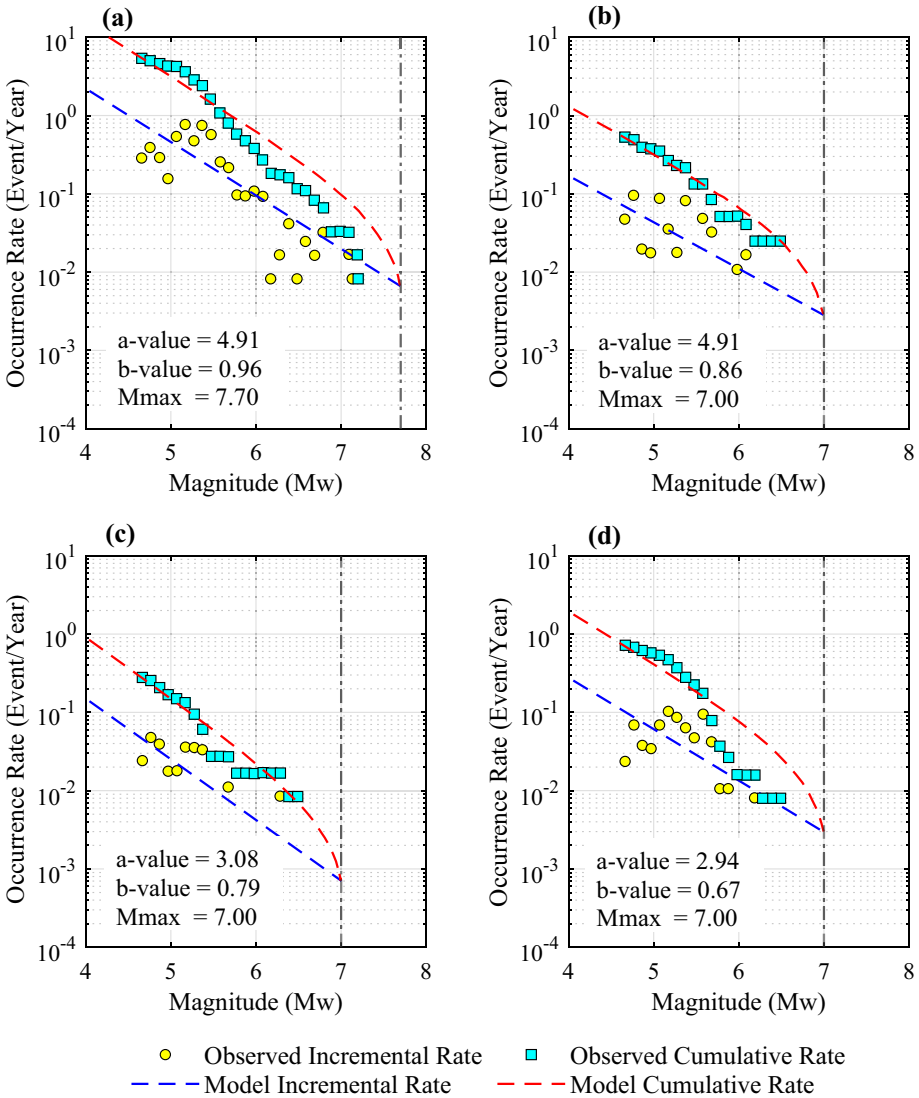


Fig. 10 Gutenberg-Richter magnitude occurrence relationships for each of the four tectonic categories or groups: **a** Category A (WRS); **b** Category B (RFB); **c** Category C (ERS); and **d** Category D (CUT) craton or the Precambrian basement of Uganda

seismic source of interest (Weatherill 2014). A truncated Gutenberg and Richter (1944) model and/or other non-parametric methods based on observed seismicity are normally used to estimate M_{max} . Subsequently, Kijko (2004) made various assumptions and suggested three models (fixed b -value, uncertain b -value, and non-parametric Gaussian) for estimating M_{max} . Many statistical methods and Bayesian approaches are well-suited for estimating the largest potential earthquake for regional data representing areal sources (Baker et al. 2021). However, because of the lack of information relating to Uganda’s seismogenic depth potential and active fault characteristics (e.g., rupture lengths, rupture

widths and slip rates), it is challenging to estimate maximum magnitudes using source-scaling relationships. Consequently, M_{max} values (shown in Table 3 and Fig. 10a–d) are arbitrarily determined by adding a conservative increment of 0.5 magnitude units to the maximum observed magnitude for each ASZ.

7 Ground motion characterisation for Uganda

A comprehensive PSHA requires suitable models for predicting the probability distribution of ground motion intensities by considering all possible rupture scenarios (Baker et al. 2021; Kramer 1996). Empirical GMPEs which are specifically developed for the region of interest should preferably be used in hazard calculations. Unfortunately, the substantial lack of reliable GMPEs for Uganda and the adjacent areas may be attributed to the absence of sufficient strong ground motion data (Bwambale et al. 2015; Poggi et al. 2017). Accordingly, Twesigomwe (1997) used a semi-theoretical approach to develop a GMPE (Eq. 4) by calibrating earthquake data and assuming a range of standard deviations as suggested by Krinitzsky et al. (1988):

$$\ln PGA = 2.832 + 0.886M_s - \ln R - 0.0027R + \ln(\epsilon) \tag{4}$$

where PGA is the peak ground acceleration (in g), M_s is the surface-wave magnitude, R is the epicentral distance (in km), and ϵ is the normally distributed error.

Furthermore, highlighting strong ground motion data gaps for the region, Mavonga (2007a) used small magnitude earthquake data to simulate strong motions of large magnitude earthquakes, and derived a GMPE (Eq. 5) for events $\geq 7.0 M_w$ and occurring in Kivu province:

$$\ln PGA = 0.152 + 1.43 M_w - 1.3 \ln R \tag{5}$$

where M_w is moment magnitude. However, seismic hazard estimates obtained using the GMPE suggested by Mavonga (2007a) may not be highly reliable because their derivation was not calibrated against actual strong ground motion data for the Kivu province.

Conversely, Pankow and Pechmann (2006) used existing strong motion records to adopt an extensional tectonic regime relationship described in Eq. (6). In this GMPE, the parameter Γ represents the site class; in which rock sites with soil depths less than 5 km, $\Gamma = 0$ and $\Gamma = 1$ for alternative site conditions (Douglas 2021).

$$\log PGA = 0.237 + 0.229(M_w - 6) - 1.052 \log D + 0.174\Gamma \tag{6}$$

where $D = \sqrt{r_{jb}^2 + h^2}$ in which r_{jb} is the Joyner-Boore distance, and $h = 7.27$ km.

In a hazard study of the Albertine region, these three GMPEs presented in Eqs. (4), (5), and (6) were compared and significant variations in the predicted PGA values were noted (Bwambale et al. 2015). The study observed that the GMPE proposed by Pankow and Pechmann (2006) gives more realistic predictions, possibly because it is derived based on strong ground motion records. In another study, Poggi et al. (2017) employed the simple functionalities embedded in the Ground Motion Toolkit (GMTK) (Weatherill et al. 2014) to select four GMPEs developed based on strong ground motion data. Although these equations are not specifically developed for SSA, they were adopted because of similar seismo-tectonic settings. In their study, Poggi et al. (2017) selected two GMPEs proposed by Akkar et al. (2014) and Chiou and Youngs (2014) for regions of active shallow crust; whilst ground motion responses

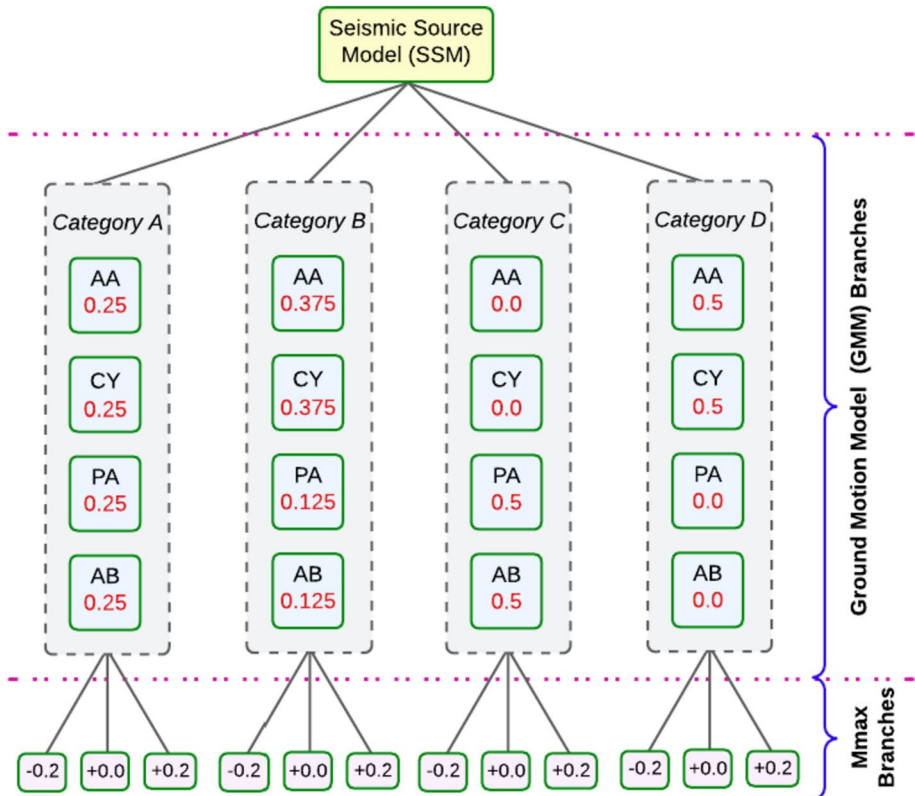


Fig. 11 Schematic diagram showing the logic tree implemented in the stochastic event-based PSHA for Uganda. Four GMPEs are used: AA—Akkar et al. (2014), CY—Chiou and Youngs (2014), PA—Pezeshk et al. (2011), and AB—Atkinson and Boore (2006) and their weights (in red) assigned

in stable continental tectonic regions were predicted using the two GMPEs derived by Pezeshk et al. (2011) and Atkinson and Boore (2006).

In this work, all four GMPEs are adopted, and a logic-tree (Fig. 11) approach is used to assign weights depending on the likelihood of each clustered tectonic type. This approach allows for the determination of confidence intervals of the predicted ground motion intensity (Bommer et al. 2005; Scherbaum et al. 2005), in addition to offering a realistic assessment of any drawbacks. Consequently, a logic-tree is implemented to minimise epistemic uncertainty associated with the present hazard model. An additional branching level is incorporated to cater for uncertainties that may arise when defining M_{max} . The number of logic tree parameters can be reduced by use of a MC-based PSHA since source zone geometries and characteristic magnitudes are initially randomized when generating synthetic catalogues (Sianko et al. 2020).

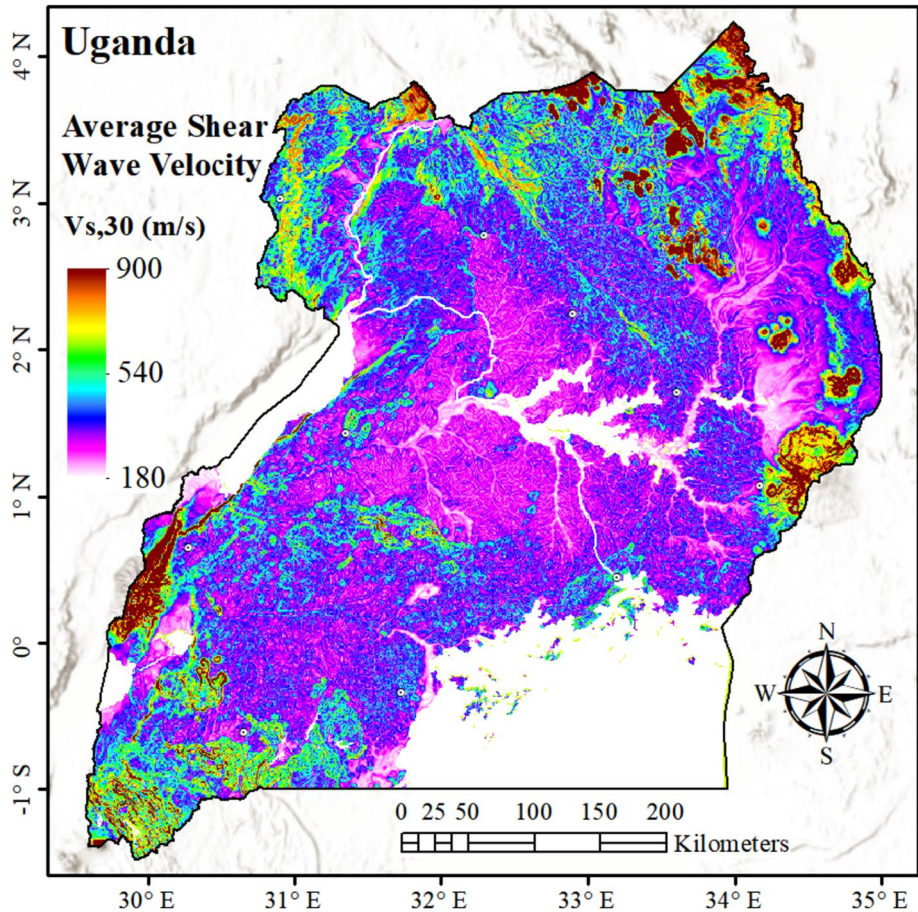


Fig. 12 Reference map showing the average shear-wave velocity in the upper 30 m of soil, used to characterise site conditions in MC-based PSHA for Uganda (Allen and Wald 2007)

8 MC-based PSHA results

As described in Sect. 6.1, the investigation area comprises of a mesh spacing of 2.5 km (with a total of 16,637 sites) including the buffer zone. The upper 30 m average shear-wave velocity reference data mapped in Fig. 12 is obtained from USGS database (Allen and Wald 2007) and values range between 180 and 900 m/s. As defined in Eurocode 8-1 (CEN 2004), these values mostly correspond to stiff-soil conditions. In addition to site-specific hazard maps, bedrock hazard maps are derived for free rock conditions, with a fixed 30 m average shear-wave velocity reference of 760 m/s assumed for each site of the investigation mesh.

Within a 50-year investigation time, the target ground motion intensity for calculation considers 5% damped RSA to estimate the POE of 10 and 2%, corresponding to 475- and 2475-year return periods respectively. These periods are chosen as standard return periods with the possible aim of incorporating results into the national seismic design code (US 319:2003) (UNBS 2003). Moreover, longer periods are avoided due to lack of historical

records which would affect calibration rates for large magnitude events. Ground response values are computed for intensity measure types and levels of PGA and spectral acceleration (SA) at spectral periods (T) of 0.05, 0.1, 0.5, 1.0, and 2.0 s; with a truncation level of ± 3 applied to the distribution of ground motion.

The calculation output includes mean hazard curves, mean and percentile (0.15, 0.5 and 0.85) Uniform Hazard Spectra (UHS), and disaggregation plots at some major Ugandan cities. In addition to the hazard maps produced in terms of PGA and SA, seismic response spectra for two example sites located in western Uganda (Mbarara and Fort Portal cities) are proposed in accordance to Eurocode 8-1 (CEN 2004), and compared with the spectra generated following the Uganda seismic code of practice for structural designs (US 319:2003) (UNBS 2003).

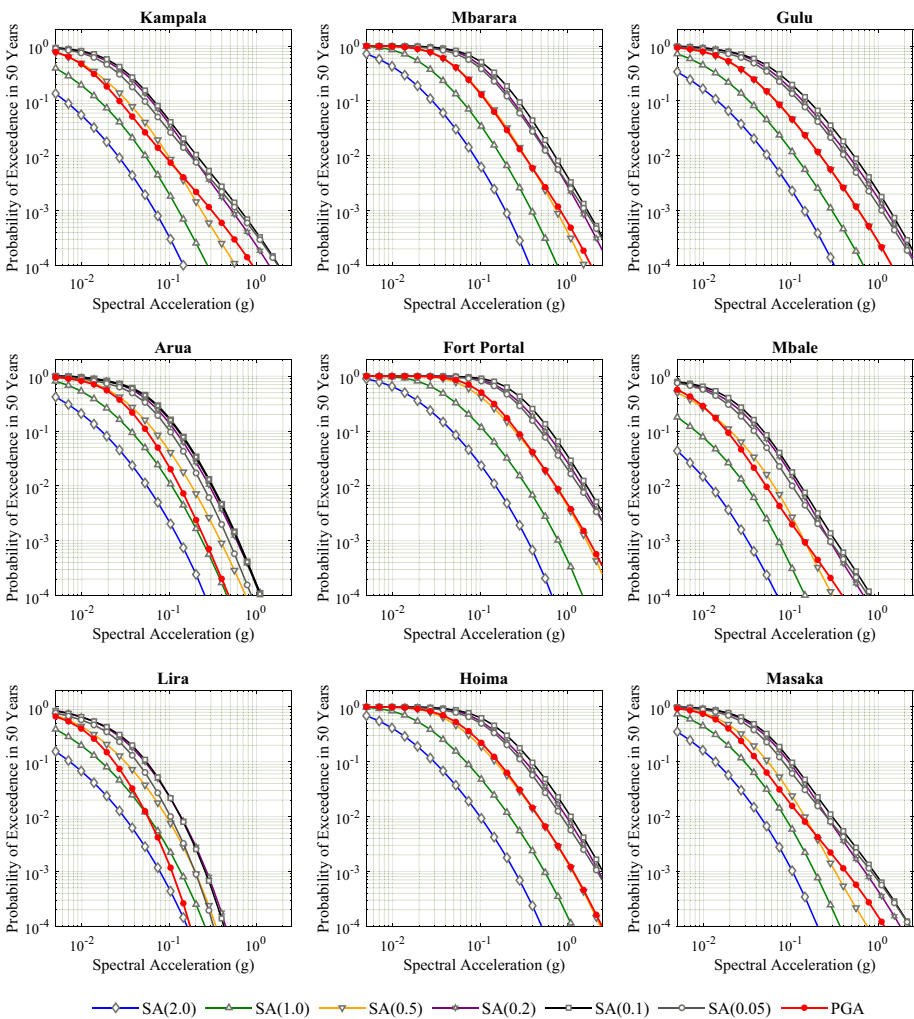


Fig. 13 Mean hazard curves calculated at various spectral periods and derived based on bedrock site conditions representing nine major cities in Uganda

8.1 Seismic hazard curves and Uniform hazard spectra

8.1.1 Mean hazard curves

In this work, mean hazard curves are computed for major cities in Uganda where earthquake risk assessment is thought necessary. Mean hazard curves for different spectral periods, presented in Fig. 13, are derived based on bedrock conditions (considering a fixed 30 m average shear-wave velocity reference of 760 m/s) at selected major regional cities. Although the concurrence of GMPEs for stable continental and active shallow crustal conditions could influence various ground motion likelihoods differently, the hazard curves seem to adequately quantify the distribution of intensity measure levels and their associated rates of exceedance.

8.1.2 Uniform hazard spectra (UHS)

Bedrock site conditions are used to compute representative mean and percentile UHS for eight major regional cities in Uganda. The mean and percentile UHS for a 10% POE in 50 years (corresponding to a 475-year return period) for eight selected cities across the country are shown in Fig. 14.

8.1.3 Comparison with previous predictions

Mean hazard curve, derived in terms of PGA, obtained for bedrock soil condition in Kampala is compared with the previous pilot study by GEM and *AfricaArray* (Poggi et al. 2017) as depicted in Fig. 15a. While Poggi et al. (2017) estimated a PGA of 0.045 g for a 10% POE in 50 years (a 475-year return period), the present model predicts a PGA of 0.027 g over the same return period. In general, differences in hazard levels range between 30 and 40% across various annual rates of exceedance. Similarly, mean UHS computed for a 10% POE in 50 years in Kampala is compared with the previous regional estimates and results plotted as shown in Fig. 15b. It can be seen that at a period of 0.1 s, the present model estimates a SA of 0.065 g whereas Poggi et al. (2017) predicted a higher value of 0.095 g. Differences in hazard results can be attributed to the fact that the model developed by Poggi et al. (2017) assumed a lower fixed 30 m average shear-wave velocity reference of 600 m/s, as opposed to bedrock conditions which are considered in the present study.

8.2 Earthquake hazard maps

8.2.1 Hazard maps in terms of peak ground acceleration (PGA)

Using refined grids, seismic hazard maps are produced for the entire country. Figure 16a, b shows the site-dependent hazard maps produced in terms of PGA for 10 and 2% exceedance probabilities, both in 50 years. As expected, the Albertine, Rwenzori and Upper Kivu regions (Zones 3 and 4 in Fig. 5) can reach a maximum PGA of 0.34 and 0.5 g in 475- and 2475-year return periods respectively; whereas the rest of the country has relatively lower accelerations. In addition, bedrock hazard maps showing PGA predictions corresponding to a 475- and 2475-year return periods are presented in Fig. 17a, b. Within a 50-year investigation time, maximum bedrock PGAs of 0.27 and 0.5 g are predicted for 10 and 2% annual exceedance rates respectively.

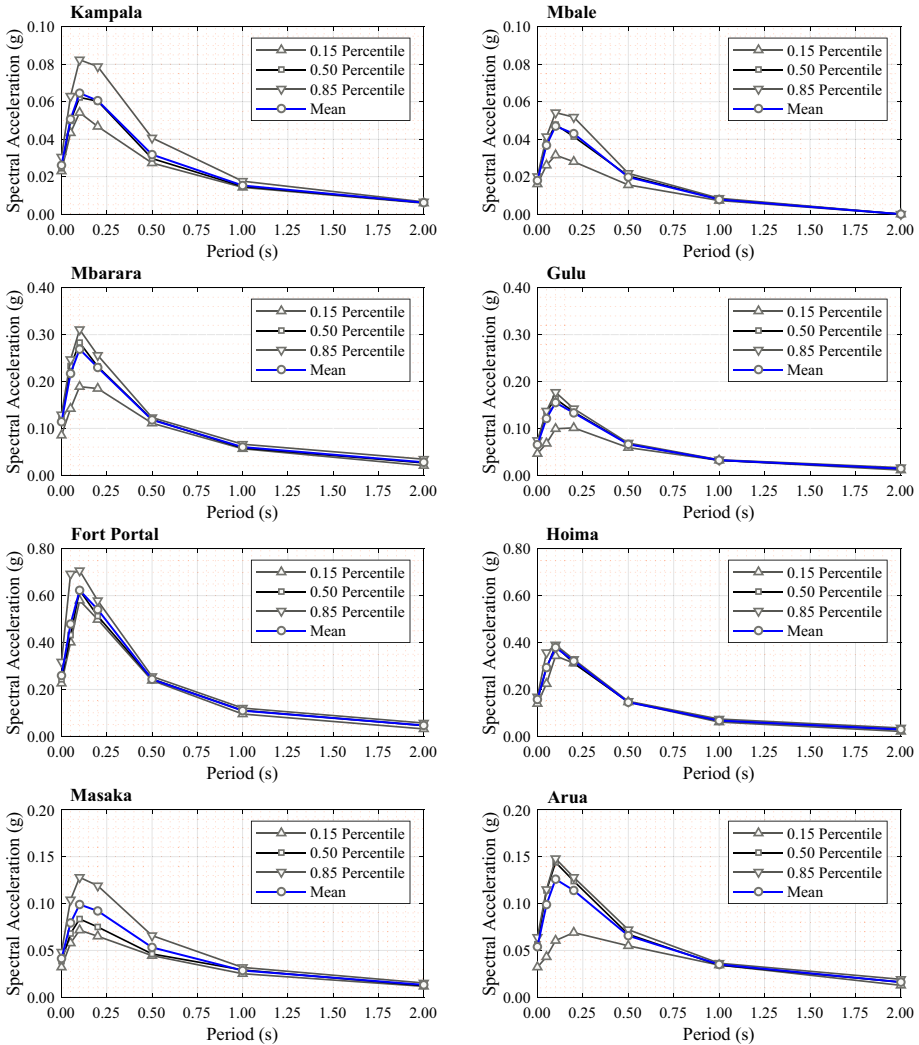


Fig. 14 Mean and percentile Uniform Hazard Spectra (UHS) based on bedrock site conditions and computed for 10% POE in 50 years (475-year return period) for eight major regional cities in Uganda

Considering a 10% annual exceedance rate in 50 years, the site-dependent hazard model (see Fig. 16a) predicts a maximum PGA of 0.34 in Fort Portal city. For the same city, the bedrock hazard model (see Fig. 17a) estimates PGA values raising to 0.255 g. Although similar soil/rock conditions may prevail throughout a city, site-dependent hazard estimates may be different due to changing local site conditions. Subsequently, this work considers bedrock hazard predictions to be more representative. Given the recent population growth, urbanisation and increased economic activity in western Uganda (that led to the creation of regional cities like Mbarara, Fort Portal and Hoima), the overall risk has significantly increased.

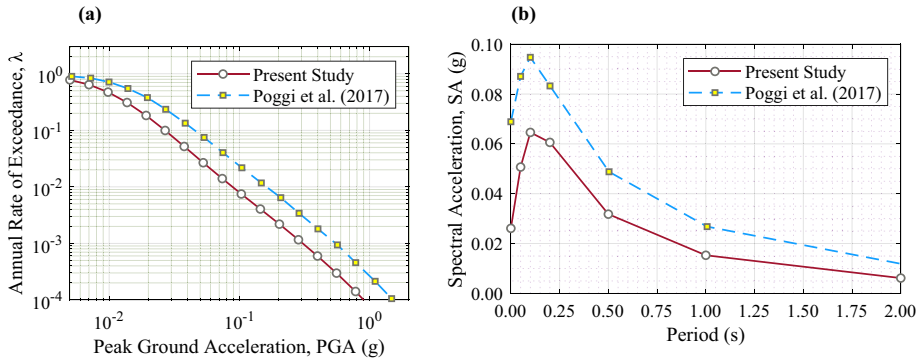


Fig. 15 Comparison of hazard results obtained in this work for an example site located in Kampala with those derived in the previous study by Poggi et al. (2017): **a** mean hazard curve in terms of PGA, and **b** mean uniform hazard spectra computed for a 10% POE in 50 years

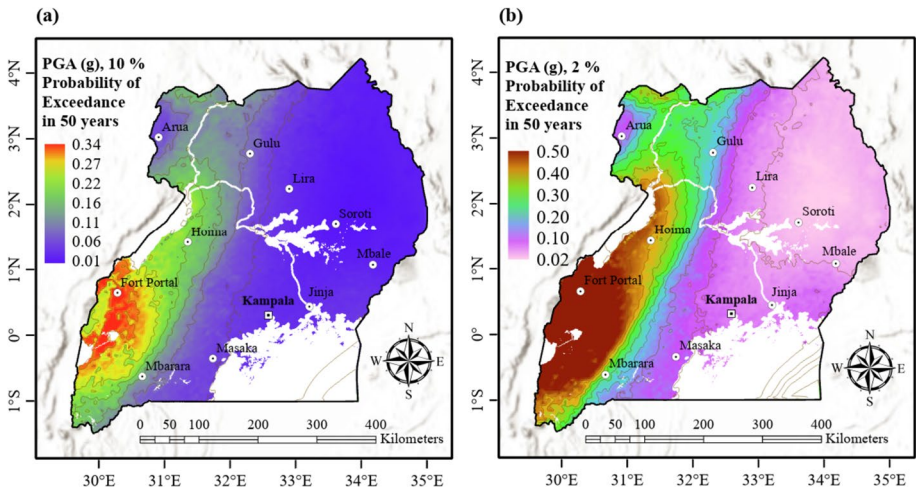


Fig. 16 Site-dependent seismic hazard maps of Uganda investigated over 50 years, in terms of PGA (g) and computed for: **a** 10% POE (475-year return period), and **b** 2% POE (2475-year return period). The contour lines are imposed on the maps at 0.05 g contour interval

8.2.2 Hazard maps in terms of spectral acceleration (SA)

For engineering applications, such as definition of seismic action in building codes, hazard maps are normally produced in terms of SA at various spectral periods. For instance, Figs. 18a–d and 19a–d respectively show the site-specific and bedrock earthquake hazard maps in terms of SA (g) at various spectral periods, T (s) which have been computed for 10% POE in 50 years (475-year return period). Whilst moderate ground shaking at various spectral periods are expected in western Uganda, majority of the country can expect SAs less than 0.1 g.

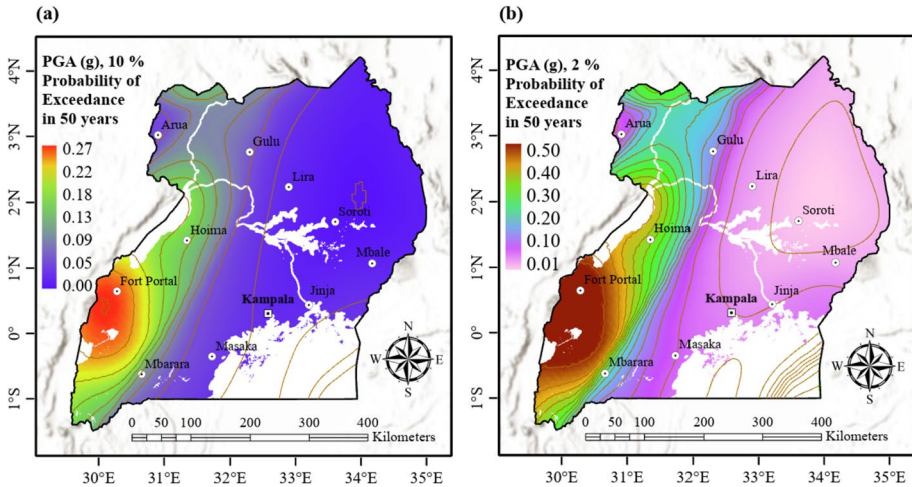


Fig. 17 Bedrock earthquake hazard maps of Uganda investigated in terms of PGA (g) and computed for: **a** 475-year return period (10% POE in 50 years), and **b** 2475-year return period (2% POE in 50-years). The contour lines are imposed on the maps at 0.03 g contour interval

8.3 Deaggregation

On completion of PSHA computations, a fundamental task is to identify the design earthquake at a particular site of interest through the process of earthquake disaggregation (Baker et al. 2021; Bazzurro and Allin Cornell 1999; McGuire 1995). In this procedure, all seismic events producing a given target hazard level for a given return period are extracted. The short-term and long-term seismic disaggregation plots are shown in Figs. 20a–c and 21a–c respectively. These plots show the contribution of sources, with different magnitude–distance measurements, to the PGA overall bedrock hazard at specific sites located in Uganda’s hazard-prone cities.

8.4 Seismic response spectra

In accordance with the provisions of Eurocode 8-1 (CEN 2004), typical elastic acceleration response spectra are developed for two example cities (Mbarara and Fort Portal). Based on the magnitudes of earthquakes generated from seismic sources, Type 1 (high seismicity) spectrum is assumed for both cities. Considering the parameters and stratigraphic profiles defined in Eurocode 8-1 (CEN 2004), the sites are classified as Type A (rock) ground. Over a 475-year return period, reference bedrock PGA values of 0.122 and 0.255 g are considered for Mbarara and Fort Portal respectively (Fig. 17a), and a damping ratio of 5% is assumed herein. For application in design of ductile structures, inelastic behaviour is explicitly taken into account by the behaviour factor derived in accordance to Eurocode 8-1 (CEN 2004). Considering the high seismic vulnerability of buildings across Uganda, low ductility class (DCL) is selected for two example sites and a behaviour factor of 1.5 is used to subsequently derive design response spectra for sites situated in Mbarara and Fort Portal. In addition to spectral displacements, the corresponding elastic and design spectral

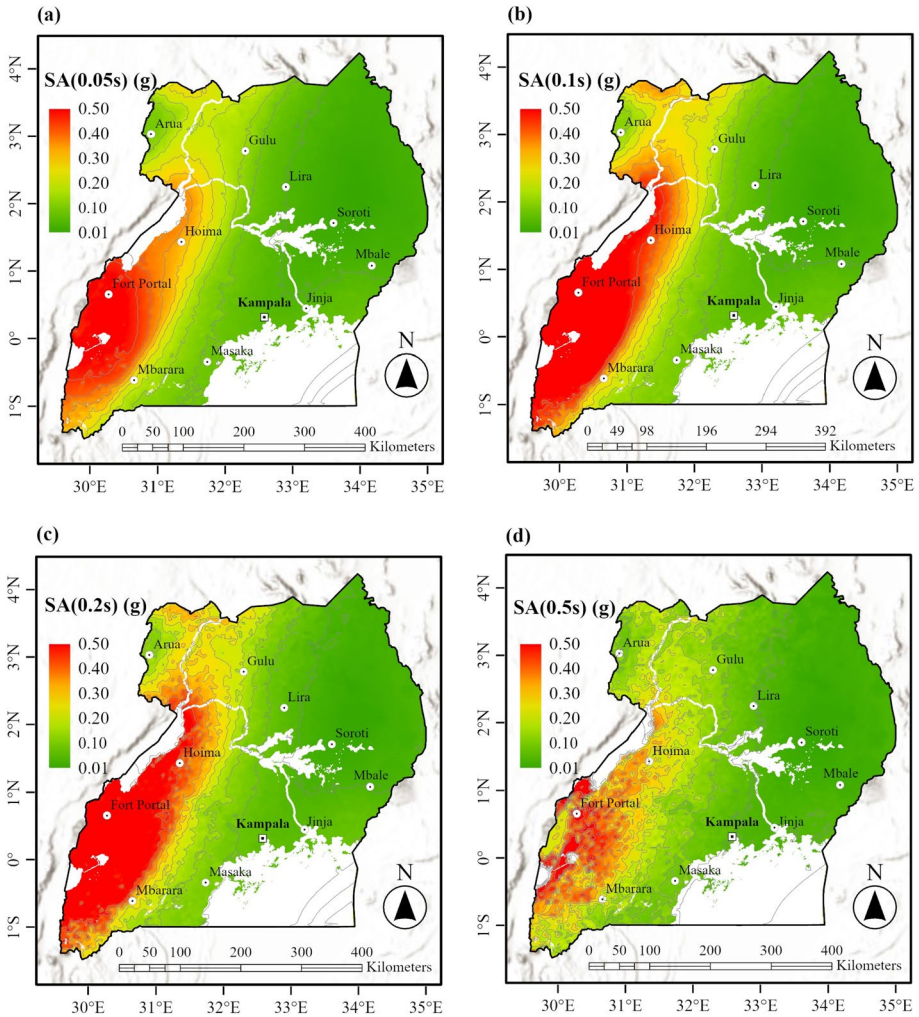


Fig. 18 Site-specific seismic hazard maps of Uganda in terms of spectral acceleration SA (g), computed for 10% probability of exceedance in 50 years (475 year return period) and at various spectral periods T (s): **a** SA(T=0.05 s), **b** SA(T=0.1 s), **c** SA(T=0.2 s), and **d** SA(T=0.5 s). The contour lines are imposed on the maps at 0.05 g contour interval

pseudo-accelerations representing seismic action in the horizontal direction in selected sites at Mbarara and Fort Portal are respectively presented in Figs. 22a, b.

As subsequently shown in Fig. 23a, b, the design pseudo-acceleration spectra derived according to Eurocode 8-1 (CEN 2004) are compared with design spectra computed based on the Uganda seismic code of practice for structural designs (US 319:2003) developed by UNBS (2003). According to the structural performance classes and importance factors described in US 319:2003 (UNBS 2003), minimal ductility in buildings of minor importance is assumed. Depending on the local ground accelerations defined in US 319:2003 (UNBS 2003), Mbarara and Fort Portal cities fall within Zone 1. However, the present

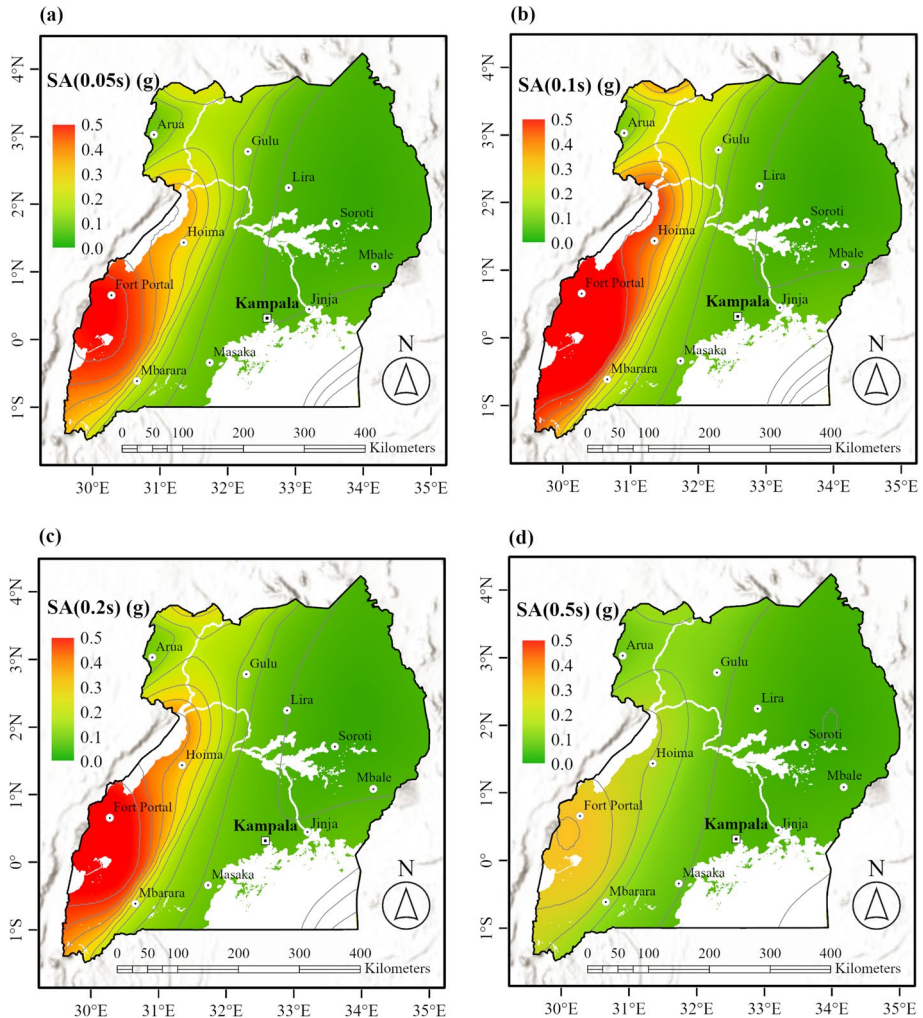


Fig. 19 Bedrock earthquake hazard maps of Uganda in terms of spectral acceleration SA (g), computed for 10% probability of exceedance in 50 years (475 year return period) and at various spectral periods T (s): **a** SA($T=0.05$ s), **b** SA($T=0.1$ s), **c** SA($T=0.2$ s), and **d** SA($T=0.5$ s). The contour lines are imposed on the maps at 0.05 g contour interval

study indicates that whereas Fort Portal is correctly located in Zone 1, the PGA map presented in Fig. 17a shows that Mbarara has lower PGA values than those given in US 319:2003 (UNBS 2003) and therefore Mbarara should fall within Zone 2.

Based on the provisions of US 319:2003 (UNBS 2003), a comparison of design spectra for Mbarara (shown in Fig. 23a) indicates that the ordinates of design spectrum obtained by considering Zone 2 conditions match Eurocode 8-1 (CEN 2004) design pseudo-acceleration spectrum better than when Zone 1 conditions are assumed. Hence, there is need to update the current seismic zones and zoning factors described in US 319:2003 (UNBS 2003) based on more accurate local ground accelerations derived in the present study. Additionally, the shape

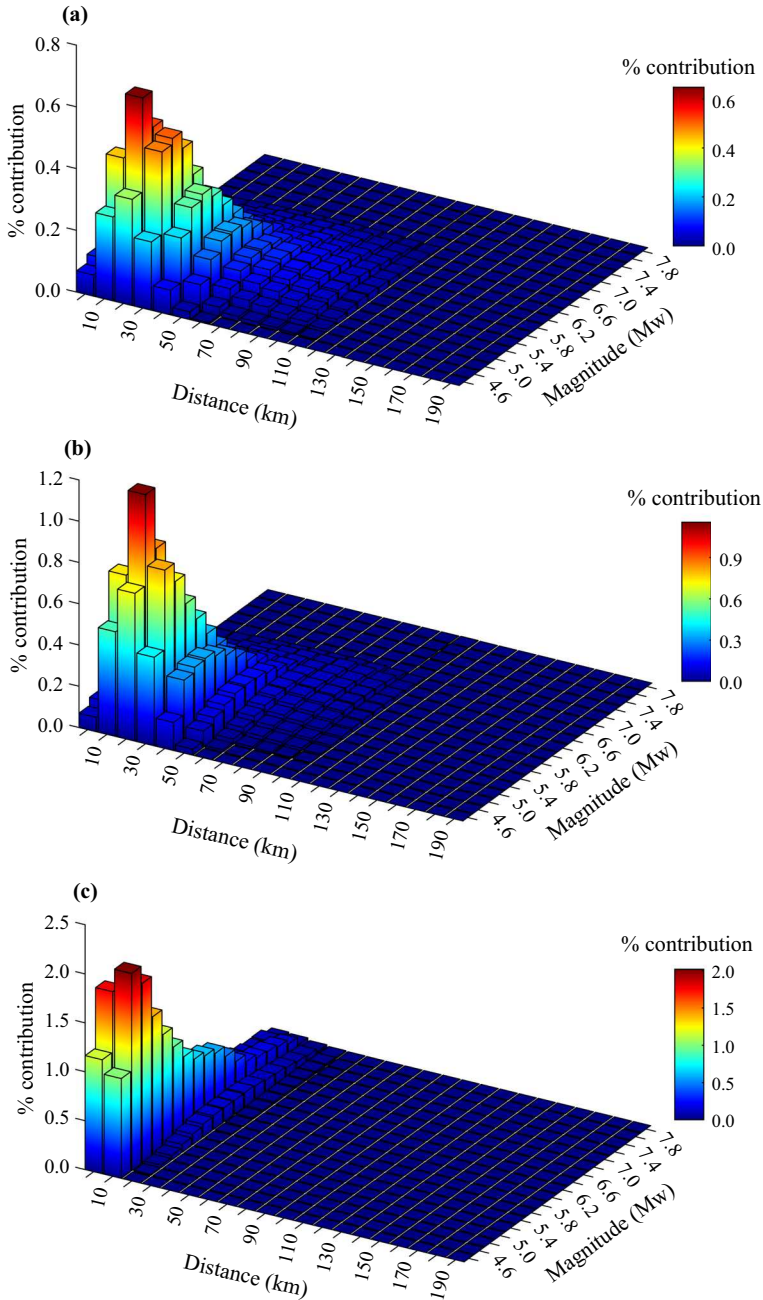


Fig. 20 Short-term earthquake disaggregation plots showing the contribution of sources, with different magnitude (M_w)—distance (km) measurements, to the PGA overall bedrock hazard for a 10% POE in 50 years (475-year return period); at specific locations in three major regional cities of Uganda: **a** Kampala, **b** Masaka, and **c** Fort Portal (high hazard region in western Uganda)

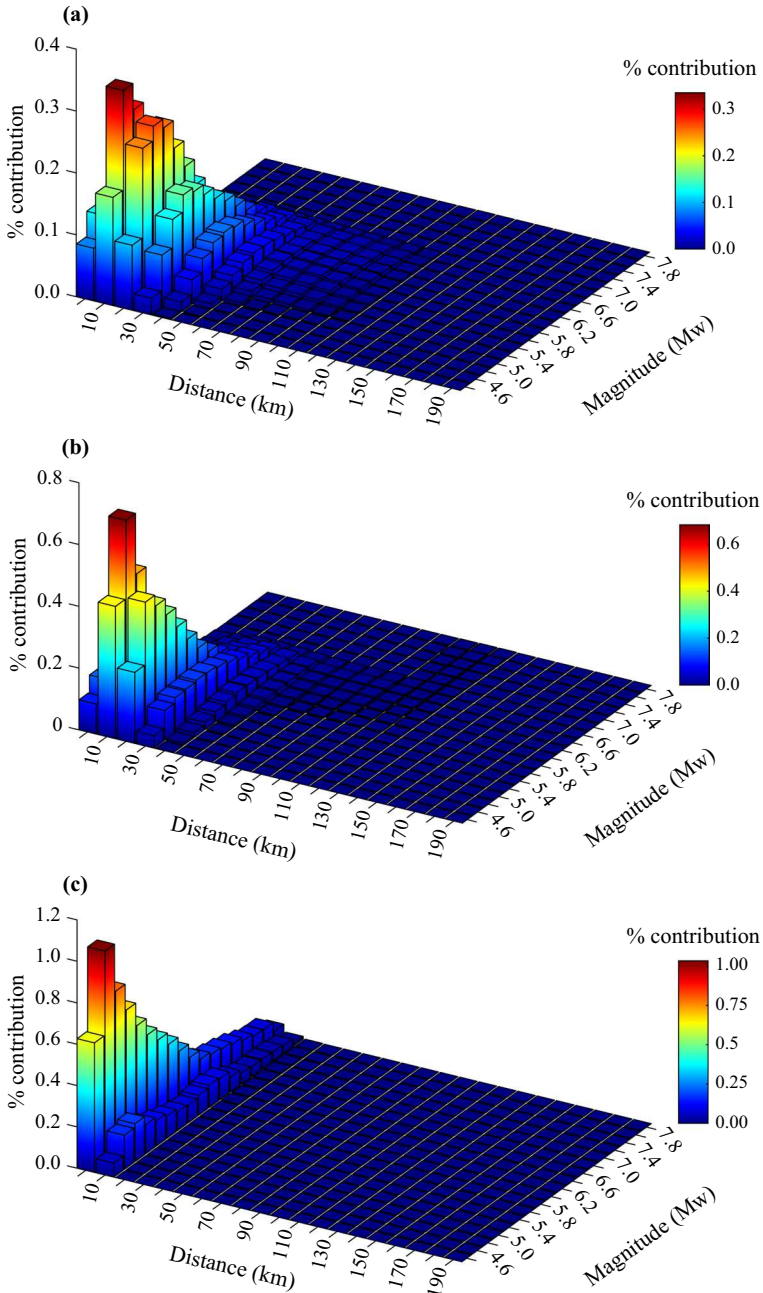


Fig. 21 Long-term earthquake disaggregation plots showing the contribution of sources, with different magnitude (M_w)—distance (km) measurements, to the PGA overall bedrock hazard for a 2% POE in 50 years (2475-year return period); at specific locations in three major regional cities of Uganda: **a** Kampala, **b** Masaka, and **c** Fort Portal (high hazard region in western Uganda)

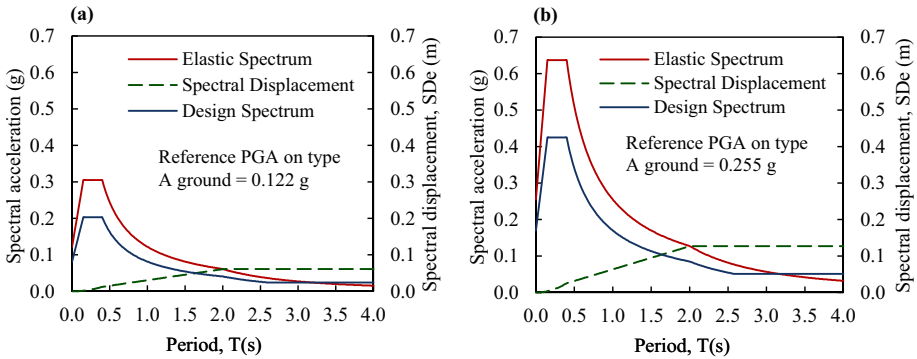


Fig. 22 Elastic spectral pseudo-acceleration, spectral displacement and design pseudo-acceleration response spectrum derived based on Eurocode 8-1 (CEN 2004). High seismicity spectrum is assumed for typical structures of low ductility class (DCL) with a 5% damping ratio and in type A (rock) ground for two selected sites located in: **a** Mbarara city, and **b** Fort Portal city

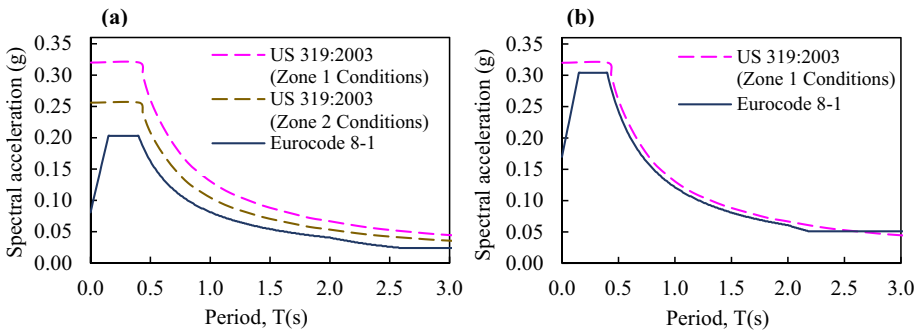


Fig. 23 Comparison of design pseudo-acceleration spectra derived according to Eurocode 8-1 (CEN 2004) with the design spectra based on US 319:2003 (UNBS 2003), for two selected example sites located in: **a** Mbarara city, and **b** Fort Portal city

of the elastic response spectrum described in US 319:2003 (UNBS 2003) should be aligned to modern seismic design codes, such as Eurocode 8-1 (CEN 2004), which explicitly consider the magnitude of earthquakes that contribute most to seismic hazard. On the other hand, design spectral pseudo-accelerations in Fort Portal city, generated according to Eurocode 8-1 (CEN 2004), closely match with the ordinates obtained following US 319:2003 (UNBS 2003) as shown in Fig. 23b. Although several assumptions are made to define behaviour factors considered in US 319:2003 (UNBS 2003), the design spectra derived according to Eurocode 8-1 (CEN 2004) generally predict lower spectral accelerations compared with the design spectra computed using US 319:2003 (UNBS 2003).

9 Discussion

Despite the limited pool of seismic hazard studies conducted for Uganda, the MC-based PSHA model developed herein is largely consistent with previous regional studies, reviewed in Sect. 2. Considering the bedrock hazard map representing a 10% POE in

50 years (see Fig. 17a), comparison of the findings with those of previous studies confirms that the country is prone to seismic hazard of varying degrees. To begin with the north-western part of Uganda, the PGA observed around Arua city is in the range of 0.03 to 0.09 g and this value closely matches the predictions from previous works like the GSHAP model (Midzi et al. 1999). The level of ground shaking increases further southwards, where for instance PGA values between 0.135 and 0.165 g can be expected in the Albertine region. Particularly, Hoima city can expect a PGA raising to 0.15 g. Although this value is consistent with the prediction by Bwambale et al. (2015) who reported a PGA of 0.152 g along the Albertine graben, it is contrary to the GEM and *AfricaArray* pilot study (Poggi et al. 2017) which reported a higher PGA value of 0.2 g. Even though these values are still moderately low, greater accelerations are observed further south towards the Rwenzori and Kigezi regions.

As depicted in Fig. 17a, the largest PGA across the country is observed along the Rwenzori rift downwards through the Lakes George and Edward. Within this region, Fort Portal city can expect a maximum acceleration ranging between 0.24 and 0.27 g over a 475-year return period. This finding is similar to the predictions from previous projects (e.g., Cheriberi and Yee 2022; Midzi et al. 1999; Poggi et al. 2017 and Twesigomwe 1997) which conclusively indicate that this region is exposed to the highest risk. However, accelerations tend to decrease further downwards (south-western Uganda); for instance the seismic hazard model proposed in this work predicts a PGA in the range of 0.09 to 0.15 g around Mbarara city. It is noted, in Fig. 17a, that ground accelerations generally decrease as one moves away from Uganda's western border. In general, the other parts of the country are prone to relatively lower seismic hazard, except for a few major cities like Gulu and Masaka where ground acceleration between 0.05 and 0.08 g can be expected. Regions around the other major regional cities like Kampala, Lira and Mbale cities can experience low PGA values less than 0.03 g. In overall, Fig. 17a, b shows that high hazard regions (e.g., Fort Portal city) can expect PGA values increasing to 0.27 g and 0.5 g over 475- and 2475-year return periods respectively. Compared with the GEM and *AfricaArray* pilot study of Poggi et al. (2017) which predicted PGA values in excess of 0.3 g over a 475-year return period, the present model estimates lower accelerations with a maximum PGA of 0.27 g over the same return period (Fig. 17a). This can be attributed to the fact that whereas bedrock conditions are adopted in the present study, Poggi et al. (2017) assumed a lower fixed 30-m average shear-wave velocity reference of 600 m/s.

Mean and percentile UHS for major Ugandan cities shown in Fig. 14 indicate that a maximum mean SA of 0.623 g at a period of 0.1 s can be expected in Fort Portal. For the same spectral period, many of the other cities can expect mean SAs less than 0.1 g, except Arua, Gulu, Mbarara and Hoima cities, where mean SAs of 0.126 g, 0.155 g, 0.269 g and 0.379 g are predicted, respectively. On the other hand, short-term bedrock earthquake disaggregation results shown in Fig. 20a–c show that corresponding design PGAs in Kampala, Masaka and Fort Portal cities are most likely to be produced by a modal earthquake of 4.6 M_w , striking at approximate distances of 20, 15 and 10 km respectively. In addition, long-term disaggregation plots presented in Fig. 21a–c indicate that a modal earthquake of 4.6 M_w , striking within 5, 10 and 15 km respectively correspond to the design PGAs in Fort Portal, Masaka and Kampala. Such information may not only be used as input parameters for assessing secondary hazards due to earthquakes, but also relevant in the selection of appropriate time-history earthquake records necessary for dynamic analysis of structures located in earthquake-prone regions.

Although the hazard model for Uganda presented herein broadly agrees with previous national and regional assessments, the major challenge however is the lack of strong

ground motion data required to determine GMPEs for the region. The model developed in this work relies on GMPEs developed for regions of similar seismo-tectonics. Yet, predicting seismic hazard using locally calibrated GMPEs would generally give more representative results. This study, therefore, recommends that potentially hazardous sites be monitored by installing new stations to record strong ground movement, as a prerequisite for deriving suitable GMPEs. This will not only aid the development of seismic response models, but also become a precursor to microzonation and hazard investigations in scenario cities across Uganda. Further challenges were faced in completeness analysis of earthquake catalogues largely due to data deficiencies, especially historical records. Therefore, the DGSM under MEMD should aim to strengthen the seismic networks within the region.

10 Conclusions

This paper presents a novel stochastic event-based PSHA model for Uganda based on a fault-oriented spatially distributed seismicity approach. An updated earthquake catalogue for the region is compiled and merged from various credible sources prior to the refinement process. Seismic source zones are delineated based on past regional seismicity, geology and seismo-tectonic environment. The zonation is preceded by employing a maximum likelihood algorithm to estimate earthquake recurrence parameters. Notwithstanding the non-existence of GMPEs specifically developed based on actual strong ground motion data for the region, a logic-tree approach is implemented to predict ground motion response using four selected GMPEs developed for regions of similar geology and seismo-tectonics. Mean hazard curves, UHS and disaggregation are derived for some major cities in Uganda. In addition to hazard maps produced in terms of PGA for 10 and 2% POE in 50 years, spectral acceleration maps at spectral periods of 0.05, 0.1, 0.2, and 0.5 s are computed for a 475-year return period. Furthermore, the design spectral pseudo-accelerations representing seismic actions in the horizontal direction are developed for two example sites in Mbarara and Fort Portal cities. The findings, which are largely consistent with previous regional studies, confirm that western Uganda is exposed to the highest level of seismicity. For example, Rwenzori and Kigezi regions can expect PGA values between 0.24 and 0.27 g, with an estimated maximum value raising to 0.255 g in Fort Portal city over a 475-year return period. Except for Hoima and Mbarara cities where maximum PGA values ranging between 0.09 and 0.165 g are predicted, the rest of the country's territory is prone to PGA values below 0.09 g. The seismic hazard assessment framework presented in this work can reliably be used as a starting point for the update and continuous improvement of a more robust seismic design code; as a step toward a more resilient built environment owing to reduced earthquake-related losses across the country.

Acknowledgements The authors are entirely responsible for the contents herein and special thanks goes to the DGSM under MEMD who provided the initial earthquake data for Uganda.

Author contributions All authors contributed to the study conception and design. Data collection was performed by MO and Dr ZO. The development of codes and analyses were performed by MO. Outputs were checked by Dr ZO and Professor KP. The first draft of the manuscript was written by MO, and Dr ZO and Professor KP commented on previous versions of the manuscript. All authors have read and approved the final manuscript.

Funding This study been made possible by funding from the United Kingdom Commonwealth Scholarship Commission (CSC).

Open Access This article is licensed under a Creative Commons Attribution 4.0 International License, which permits use, sharing, adaptation, distribution and reproduction in any medium or format, as long as you give appropriate credit to the original author(s) and the source, provide a link to the Creative Commons licence, and indicate if changes were made. The images or other third party material in this article are included in the article's Creative Commons licence, unless indicated otherwise in a credit line to the material. If material is not included in the article's Creative Commons licence and your intended use is not permitted by statutory regulation or exceeds the permitted use, you will need to obtain permission directly from the copyright holder. To view a copy of this licence, visit <http://creativecommons.org/licenses/by/4.0/>.

References

- Aki K (1965) Maximum likelihood estimate of b in the formula $\log N = a - bM$ and its confidence limits. *Bull Earthq Res Inst Univ Tokyo* 43:237–239
- Akkar S, Sandikkaya MA, Bommer JJ (2014) Empirical ground-motion models for point-and extended-source crustal earthquake scenarios in Europe and the Middle East. *Bull Earthq Eng* 12(1):359–387
- Alamilla JL, Vai R, Esteva L (2015) Completeness assessment of earthquake catalogues under uncertain knowledge. *J Seismolog* 19(1):27–40
- Albaric J, Perrot J, Déverchère J, Deschamps A, Le Gall B, Ferdinand R, Petit C, Tiberi C, Sue C, Songo M (2010) Contrasted seismogenic and rheological behaviours from shallow and deep earthquake sequences in the North Tanzanian Divergence, East Africa. *J Afr Earth Sci* 58(5):799–811
- Albini P, Musson R, Gomez Capera A, Locati M, Rovida A, Stucchi, M, and Viganò D (2013) Global historical earthquake archive and catalogue (1000–1903). Pavia, Italy
- Allen TI, Wald DJ (2007) Topographic slope as a proxy for global seismic site conditions ($V_{S,30}$) and amplification around the globe. U.S. geological survey open-file report 2007–1357. p 69
- Ambraseys N, Adams R (1991) Reappraisal of major African earthquakes, south of 20° N, 1900–1930. *Nat Hazards* 4(4):389–419
- Asefa J, Ayele A (2021) Seismicity of the East African rift system for the period 2013 to 2016. *J Afr Earth Sci* 183:104315
- Atkinson GM, Boore DM (2006) Earthquake ground-motion prediction equations for eastern North America. *Bull Seismol Soc Am* 96(6):2181–2205
- Baker J, Bradley B, Stafford P (2021) *Seismic hazard and risk analysis*. Cambridge University Press, Cambridge
- Baker BH, Mohr PA, and Williams LAJ (1972) *Geology of the eastern rift system of Africa*
- Balikudembe JK and Sinclair P (2018) Uganda at glance of 5.7 magnitude earthquake: lessons for earthquake risk reduction. *PLoS Curr* 10
- Bazzurro P, Allin Cornell C (1999) Disaggregation of seismic hazard. *Bull Seismol Soc Am* 89(2):501–520
- Bender B (1983) Maximum likelihood estimation of b values for magnitude grouped data. *Bull Seismol Soc Am* 73(3):831–851
- Bisset C (1945) Notes on earth tremor on and about 18 March 1945. *Bull Uganda Soc* 4:25–28
- Bommer JJ (2022) Earthquake hazard and risk analysis for natural and induced seismicity: towards objective assessments in the face of uncertainty. *Bull Earthq Eng* 20(6):2825–3069
- Bommer JJ, Scherbaum F, Bungum H, Cotton F, Sabetta F, Abrahamson NA (2005) On the use of logic trees for ground-motion prediction equations in seismic-hazard analysis. *Bull Seismol Soc Am* 95(2):377–389
- Boyd OS (2012) Including foreshocks and aftershocks in time-independent probabilistic seismic-hazard analyses. *Bull Seismol Soc Am* 102(3):909–917
- Brazier RA, Nyblade AA, and Florentin J (2005) Focal mechanisms and the stress regime in NE and SW Tanzania, East Africa. *Geophys. Res Lett* 32(14)
- Brzev S, Scawthorn C, Charleson AW, Allen L, Greene M, Jaiswal K, and Silva V (2013) *GEM building taxonomy (Version 2.0)*
- Bustos A, Guillermo (2009). An exploratory study of parameter sensitivity, representation of results and extensions of PSHA: case study-United Arab Emirates Imperial College London]
- Bwambale B, Bagampadde U, Gidudu A, Martini F (2015) Seismic hazard analysis for the Albertine region, Uganda—a probabilistic approach. *S Afr J Geol* 118(4):411–424
- Cahen L, Snelling N (1966) *The geochronology of equatorial Africa*. North-Holland Publishing Company, Amsterdam

- Cao A, Gao SS (2002) Temporal variation of seismic b-values beneath northeastern Japan island arc. *Geophys Res Lett* 29(9):4841–4843
- CEN (2004) Eurocode 8: design of structures for earthquake resistance, part 1: general rules. Seismic actions and rules for buildings. EN 1998-1
- Chen W-F, Scawthorn C (2003) *Earthquake engineering handbook*. CRC Press, Boca Raton, London
- Cheriberi D, Yee E (2022) Preliminary seismic hazard analyses for the Ugandan region. *Appl Sci* 12(2):598
- Chiou BS-J, Youngs RR (2014) Update of the Chiou and Youngs NGA model for the average horizontal component of peak ground motion and response spectra. *Earthq Spectra* 30(3):1117–1153
- Chorowicz J (2005) The east African rift system. *J Afr Earth Sci* 43(1–3):379–410
- Craig T, Jackson J, Priestley K, McKenzie D (2011) Earthquake distribution patterns in Africa: their relationship to variations in lithospheric and geological structure, and their rheological implications. *Geophys J Int* 185(1):403–434
- Crowley H, Bommer JJ (2006) Modelling seismic hazard in earthquake loss models with spatially distributed exposure. *Bull Earthq Eng* 4(3):249–273
- Crowley H (2005) An investigative study on the modelling of earthquake hazard for loss assessment. *Individ Study*
- Darracott BW (1974) The structure of speke gulf, tanzania, and its relation to the East African rift system. *Tectonophysics* 23(1–2):155–175
- Dawson J (1992) Neogene tectonics and volcanicity in the North Tanzania sector of the Gregory Rift Valley: contrasts with the Kenya sector. *Tectonophysics* 204(1–2):81–92
- Delvaux D, Mulumba J-L, Sebagenzi MNS, Bondo SF, Kervyn F, Havenith H-B (2017) Seismic hazard assessment of the Kivu rift segment based on a new seismotectonic zonation model (western branch, East African Rift system). *J Afr Earth Sci* 134:831–855
- DGSM (2022) The Uganda earthquake catalogue (1970 - 2022). Accessed on 18 Jan 2022 from Ministry of Energy and Mineral Development, Uganda
- Di Giacomo D, Bondár I, Storchak DA, Engdahl ER, Bormann P, Harris J (2015) ISC-GEM: global instrumental earthquake catalogue (1900–2009), III. Re-computed MS and mb, proxy MW, final magnitude composition and completeness assessment. *Phys Earth Planet Inter* 239:33–47
- Di Giacomo D, Engdahl ER, Storchak DA (2018) The ISC-GEM earthquake catalogue (1904–2014): status after the extension project. *Earth Syst Sci Data* 10(4):1877–1899
- Douglas J (2021) Ground motion prediction equations 1964–2021
- Ebinger CJ (1989) Tectonic development of the western branch of the East African rift system. *Geol Soc Am Bull* 101(7):885–903
- Edwards B, Allmann B, Fäh D, Clinton J (2010) Automatic computation of moment magnitudes for small earthquakes and the scaling of local to moment magnitude. *Geophys J Int* 183(1):407–420
- Engdahl E, Villaseñor A (2002) *International handbook of earthquake and engineering seismology*, Part A. Academic Press, London
- Ericsson U (1971) A linear model for the yield dependence of magnitudes measured by a seismographic network. *Geophys J Int* 25(1–3):49–69
- Fairhead J, Girdler R (1971) The seismicity of Africa. *Geophys J Int* 24(3):271–301
- Fairhead J, Stuart G (1982) The seismicity of the East African rift system and comparison with other continental rifts. *Cont Ocean Rifts* 8:41–61
- Felzer KR (2008) Calculating California seismicity rates (2331–1258)
- FEMA (2003) HAZUS-MH technical manual. Federal emergency management agency, Washington DC. FEMA Washington, DC
- Fernandes R, Ambrosius B, Noomen R, Bastos L, Combrinck L, Miranda J, Spakman W (2004) Angular velocities of Nubia and Somalia from continuous GPS data: implications on present-day relative kinematics. *Earth Planet Sci Lett* 222(1):197–208
- Field EH, Jordan TH, Cornell CA (2003) A developing community-modeling environment for seismic hazard analysis. *Seismol Res Lett* 74(4):406–419
- Furman T, Bryce JG, Karson J, Iotti A (2004) East African Rift System (EARS) plume structure: insights from Quaternary mafic lavas of Turkana, Kenya. *J Petrol* 45(5):1069–1088
- Furman T, Kaleta KM, Bryce JG, Hanan BB (2006) Tertiary mafic lavas of Turkana, Kenya: constraints on East African plume structure and the occurrence of high- μ volcanism in Africa. *J Pet* 47(6):1221–1244
- Gardner J, Knopoff L (1974) Is the sequence of earthquakes in Southern California, with aftershocks removed, Poissonian? *Bull Seismol Soc Am* 64(5):1363–1367
- Graves R, Jordan TH, Callaghan S, Deelman E, Field E, Juve G, Kesselman C, Maechling P, Mehta G, Milner K (2011) CyberShake: A physics-based seismic hazard model for southern California. *Pure Appl Geophys* 168(3):367–381

- Gutenberg B, Richter C (1941) Seismicity of the Earth, vol 34. Geological Society of America, Boulder
- Gutenberg B, Richter CF (1944) Frequency of earthquakes in California. *Bull Seismol Soc Am* 34(4):185–188
- Hafiez H (2015) Estimating the magnitude of completeness for assessing the quality of earthquake catalogue of the ENSN, Egypt. *Arab J Geosci* 8(11):9315–9323
- Hampton C (1995) The fort portal earthquake 5th February 1994, W Uganda. *Berl Geowiss Abh A* 175:147–158
- Hartnady C, Benavraham Z, Rogers J (1992) Deep-ocean basins and submarine rises off the continental margin of south-eastern Africa. *New Geol Res*
- Hashemi A (2017) Effects of thermal insulation on thermal comfort in low-income tropical housing. *Energy Procedia* 134:815–824
- Havskov J and Ottemöller L (2003) SEISAN: the earthquake analysis software, version 8.0. Department of Earth Science, The University of Bergen, Norway
- ISC (2022) Seismological centre, on-line bulletin. Int Seismol Cent, Thatcham, United Kingdom. <http://www.isc.ac.uk>
- Ishimoto M (1939) Observations of earthquakes registered with the microseismograph constructed recently. *Bull Earthq Res Inst* 17:443–478
- Johnson K, Pagani M (2021) Probabilistic seismic hazard analysis (PSHA) training manual. GEM Found. https://doi.org/10.13117/OQ_HAZARD_TRAINING_MANUAL
- Jónasson K, Bessason B, Helgadóttir Á, Einarsson P, Guðmundsson GB, Brandsdóttir B, Vogfjörð KS, Jónsdóttir K (2021) A harmonised instrumental earthquake catalogue for Iceland and the northern Mid-Atlantic Ridge. *Nat Hazard* 21(7):2197–2214
- Jonathan E (1996) Some aspects of seismicity in Zimbabwe and Eastern and Southern Africa. Unpublished MSc. Thesis, Institute of Solid Earth Physics, University of Bergen, Norway
- Jones A, Michael A, Simpson B, Jacob S, Oppenheimer D (2000) Rapid distribution of earthquake information for everybody. *Seismol Res Lett* 71(3):355–358
- Kahuma A, Kiggundu B, Mwakali J, Taban-Wani G (2006) Building material aspects in earthquake resistant construction in western Uganda. In: Proceedings from the international conference on advances in engineering and technology
- Kampunzu AB, Caron J-PH, Lubala RT (1986) The East African rift, magma genesis and astheno-lithospheric dynamics. *Epis J Int Geosci* 9(4):211–216
- Karp T, Scholz CA, and McGlue MM (2012) Structure and stratigraphy of the Lake Albert Rift, East Africa: observations from seismic reflection and gravity data
- Kijko A (2004) Estimation of the maximum magnitude earthquake m_{max} . *Pure Appl Geophys* 161:1–27
- Kijko A, Smit A (2012) Extension of the Aki-Utsu b-value estimator for incomplete catalogs. *Bull Seismol Soc Am* 102(3):1283–1287
- Knopoff L (2000) The magnitude distribution of declustered earthquakes in Southern California. *Proc Natl Acad Sci* 97(22):11880–11884
- Kramer SL (1996) Geotechnical earthquake engineering. Pearson Education India, Bangalore
- Krinitzsky E, Chang FK, Nuttli OW (1988) Magnitude-related earthquake ground motions. *Bull Assoc Eng Geol* 25(4):399–423
- Lazarov R and Christoskov L (1981) Statistical aspects of the magnitude-frequency relation for Bulgaria. *Anal Seism Seism Hazard* 56–66
- Loupekine, I. (1966). The Toro earthquake of 20 March 1966 and preliminary interpretation of seismograms: Uganda-(mission) 5–19 April 1966.
- Maasha N (1975) The seismicity and tectonics of Uganda. *Tectonophysics* 27(4):381–393
- MacDonald R (1966) Geological map of Uganda. Department of Geological Survey and Mines, Uganda
- Macgregor D (2015) History of the development of the East African Rift system: a series of interpreted maps through time. *J Afr Earth Sci* 101:232–252
- MATLAB (2021b) <https://uk.mathworks.com/>. Accessed May 2021
- Mavonga T (2007a) An estimate of the attenuation relationship for strong ground motion in the Kivu Province, Western Rift Valley of Africa. *Phys Earth Planet Inter* 162(1–2):13–21
- Mavonga T (2007b) Some characteristics of aftershock sequences of major earthquakes from 1994 to 2002 in the Kivu province, Western Rift Valley of Africa. *Tectonophysics* 439(1–4):1–12
- Mavonga T, Durrheim R (2009) Probabilistic seismic hazard assessment for the Democratic Republic of Congo and surrounding areas. *S Afr J Geol* 112(3–4):329–342
- McConnell R (1972) Geological development of the rift system of eastern Africa. *Geol Soc Am Bull* 83(9):2549–2572
- McDougall I, Brown FH (2009) Timing of volcanism and evolution of the northern Kenya Rift. *Geol Mag* 146(1):34–47

- McGuire RK (1995) Probabilistic seismic hazard analysis and design earthquakes: closing the loop. *Bull Seismol Soc Am* 85(5):1275–1284
- McGuire R (1996) FRISK88M: user's manual. Risk Engineering Inc., Louisville, CO, p 4155
- McGuire RK (2004) Seismic hazard and risk analysis. Earthquake Engineering Research Institute, San Francisco
- Michael AJ (1987) Use of focal mechanisms to determine stress: a control study. *J Geophys Res Solid Earth* 92(B1):357–368
- Midzi V, Hlatywayo DJ, Chapola LS, Kebede F, Atakan K, Lombe DK, Turyomurugendo G, and Tugume FA (1999) Seismic hazard assessment in Eastern and Southern Africa. *Ann Geophys*
- Midzi V, Manzunzu B (2014) Large recorded earthquakes in sub-Saharan Africa. *Extreme Nat Hazards Disaster Risks Soc Implic* 1:214
- Mignan A, Woessner J (2012) Estimating the magnitude of completeness for earthquake catalogs. *Community Online Resour Stat Seism Anal* 1–45
- Musson RM (1999) Probabilistic seismic hazard maps for the North Balkan region. *Ann Geophys*
- Muwanga A, Schuman A, Biryabarema M (2001) Landslides in Uganda—documentation of a natural hazard. *Doc Nat* 136:111–115
- NEDC (1994) Preliminary report on earthquake disaster in Kabaloro, Bundibugyo and Kasese districts. Ministry of Labour and Social Affairs, Republic of Uganda, 56
- NGDC and WDS (2022) Significant volcanic eruptions database. NOAA National Centers for Environmental Information. <https://doi.org/10.7289/V5JW8BSH>
- Nyblade AA, Langston CA (1995) East African earthquakes below 20 km depth and their implications for crustal structure. *Geophys J Int* 121(1):49–62
- Ordaz M and Salgado-Gálvez M (2017) *R-CRISIS* validation and verification document
- Pagani M, Monelli D, Weatherill G, Danciu L, Crowley H, Silva V, Henshaw P, Butler L, Nastasi M, Panzeri L (2014) OpenQuake engine: an open hazard (and risk) software for the global earthquake model. *Seismol Res Lett* 85(3):692–702
- Pagani M, Silva V, Rao A, Simonato M, and Johnson K (2023) OpenQuake engine manual
- Pankow KL, Pechmann JC (2006) The SEA99 ground-motion predictive relations for extensional tectonic regimes: revisions and a new peak ground velocity relation. *Bull Seismol Soc Am* 96(1):364–364
- Petit C, Ebinger C (2000) Flexure and mechanical behavior of cratonic lithosphere: gravity models of the east African and Baikal rifts. *J Geophys Res Solid Earth* 105(B8):19151–19162
- Pezeshk S, Zandieh A, Tavakoli B (2011) Hybrid empirical ground-motion prediction equations for eastern North America using NGA models and updated seismological parameters. *Bull Seismol Soc Am* 101(4):1859–1870
- Poggi V, Durrheim R, Tuluka GM, Weatherill G, Gee R, Pagani M, Nyblade A, Delvaux D (2017) Assessing seismic hazard of the East African Rift: a pilot study from GEM and AfricaArray. *Bull Earthq Eng* 15(11):4499–4529
- Reasenber P (1985) Second-order moment of central California seismicity, 1969–1982. *J Geophys Res Solid Earth* 90(B7):5479–5495
- Roberts EM, Stevens N, O'Connor PM, Dirks P, Gottfried MD, Clyde W, Armstrong R, Kemp A, Hemming S (2012) Initiation of the western branch of the East African Rift coeval with the eastern branch. *Nat Geosci* 5(4):289–294
- Rothé JP (1969) The seismicity of the earth, 1953–1965: la séismicité du globe 1953–1965, Vol 1. Unesco
- Rydelek PA, Sacks IS (1989) Testing the completeness of earthquake catalogues and the hypothesis of self-similarity. *Nature* 337(6204):251–253
- Rykounov L, Sedov V, Savrina L, Bourmin VJ (1972) Study of microearthquakes in the rift zones of East Africa. *Tectonophysics* 15(1–2):123–130
- Saria E, Calais E, Stamps D, Delvaux D, Hartnady C (2014) Present-day kinematics of the East African Rift. *J Geophys Res Solid Earth* 119(4):3584–3600
- Scherbaum F, Bommer JJ, Bungum H, Cotton F, Abrahamson NA (2005) Composite ground-motion models and logic trees: methodology, sensitivities, and uncertainties. *Bull Seismol Soc Am* 95(5):1575–1593
- Schlüter T (2008) Geological atlas of Africa, vol 307. Springer, New York
- Shudofsky GN (1985) Source mechanisms and focal depths of East African earthquakes using Rayleigh-wave inversion and body-wave modelling. *Geophys J Int* 83(3):563–614
- Sianko I, Ozdemir Z, Khoshkholghi S, Garcia R, Hajirasouliha I, Yazgan U, Pilakoutas K (2020) A practical probabilistic earthquake hazard analysis tool: case study Marmara region. *Bull Earthq Eng* 18(6):2523–2555
- Spooner C, Hepworth J, Fairbairn H (1970) Whole-rock Rb-Sr isotopic investigation of some east African granulites. *Geol Mag* 107(6):511–521

- Stepp J (1972) Analysis of completeness of the earthquake sample in the Puget Sound area and its effect on statistical estimates of earthquake hazard. In: Proc. of the 1st Int. Conf. on Microzonation, Seattle
- Storchak DA, Di Giacomo D, Bondár I, Engdahl ER, Harris J, Lee WH, Villaseñor A, Bormann P (2013) Public release of the ISC–GEM global instrumental earthquake catalogue (1900–2009). *Seismol Res Lett* 84(5):810–815
- Storchak DA, Di Giacomo D, Engdahl E, Harris J, Bondár I, Lee WH, Bormann P, Villaseñor A (2015) The ISC-GEM global instrumental earthquake catalogue (1900–2009): introduction. *Phys Earth Planet Inter* 239:48–63
- Styron R, Pagani M (2020) The GEM global active faults database. *Earthq Spectra* 36(1_Suppl):160–180
- Sutton GH, Berg E (1958) Seismological studies of the western rift valley of Africa. *EOS Trans Am Geophys Union* 39(3):474–481
- Sykes LR (1967) Mechanism of earthquakes and nature of faulting on the mid-oceanic ridges. *J Geophys Res* 72(8):2131–2153
- Sykes LR, Landisman M (1964) The seismicity of east Africa, the Gulf of Aden and the Arabian and Red Seas. *Bull Seismol Soc Am* 54(6A):1927–1940
- Tanaka K (1983) Seismicity and focal mechanism of the volcanic earthquakes in the Virunga Volcanic Region. *Volcanoes Nyiragongo Nyamuragira Geophys Aspects* 19–28
- Tanner P (1970) The Ruwenzori fold belt of east Africa. *Ann Rep Res Inst. African Geology University Leeds*
- Tongue J, Maguire P, Burton P (1994) An earthquake study in the Lake Baringo basin of the central Kenya Rift. *Tectonophysics* 236(1–4):151–164
- Turyomurugyendo G (1996) Some aspects of seismic hazard in East and South African region. MSc thesis, Institute of Solid Earth Physics, MSc, University of Bergen, Norway. (unpublished)
- Twesigomwe E (1997) Seismic hazards in Uganda. *J Afr Earth Sc* 24(1–2):183–195
- UBoS (2022) Statistical abstract. Ministry of Finance, Planning and Economic Development, (GoU). https://www.ubos.org/wp-content/uploads/publications/05_20232022_Statistical_Abstract.pdf
- Uhrhammer R (1986) Characteristics of northern and central California seismicity. *Earthq Notes* 57(1):21
- UNBS (2003) US 319:2003. Seismic code of practice for structural designs. Uganda National Bureau of Standards. <https://webstore.unbs.go.ug/store.php?src=1701&preview>
- USGS (2016) M5.9–22 km NE of Nsunga, Tanzania. U.S. Geological Survey—earthquake hazards Program. <http://earthquake.usgs.gov/earthquakes/eventpage/us10006nkn#executive>. Accessed 13 June 2022
- USGS (2022) Earthquake. Search earthquake catalog. URL. <https://earthquake.usgs.gov/earthquakes/search/>. Accessed 10 Jan 2022
- van Stiphout T, Zhuang J, Marsan D (2012) Seismicity declustering. *Community Online Resour Stat Seism Anal* 10(1):1–25
- Vicente R, Parodi S, Lagomarsino S, Varum H, Silva J (2011) Seismic vulnerability and risk assessment: case study of the historic city centre of Coimbra. *Portugal Bull Earthq Eng* 9(4):1067–1096
- Vilanova SP, Nemser ES, Besana-Ostman GM, Bezeghoud M, Borges JF, Brum da Silveira A, Cabral J, Carvalho J, Cunha PP, Dias RP (2014) Incorporating descriptive metadata into seismic source zone models for seismic-hazard assessment: A case study of the Azores–West Iberian region. *Bull Seismol Soc Am* 104(3):1212–1229
- Villacís CA (1999) RADIUS (Risk assessment tools for diagnosis of urban areas against seismic disasters)
- Weatherill G, Pagani M, Garcia J (2016) Exploring earthquake databases for the creation of magnitude-homogeneous catalogues: tools for application on a regional and global scale. *Geophys J Int* 206(3):1652–1676
- Weatherill G, Pagani M, Garcia J (2014) OpenQuake ground motion toolkit—user guide, global earthquake model (GEM). Technical report
- Weatherill GA (2014) OpenQuake hazard modeller’s toolkit - user guide. Global Earthquake Model (GEM). Technical Report
- Weichert DH (1980) Estimation of the earthquake recurrence parameters for unequal observation periods for different magnitudes. *Bull Seismol Soc Am* 70(4):1337–1346
- Westerhof AB, Härmä P, Isabirye E, Katto E, Koistinen T, Kuosmanen E, Lehto T, Lehtonen MI, Mäkitie H, and Manninen T (2014) Geology and geodynamic development of Uganda with explanation of the 1: 1,000,000 scale geological map. Geological survey of Finland
- Wiemer S (2001) A software package to analyze seismicity: ZMAP. *Seismol Res Lett* 72(3):373–382
- Wiemer S and Wyss M (2000) Minimum magnitude of completeness in earthquake catalogs: examples from Alaska, the western United States, and Japan. *Bulletin of the seismological society of America*
- Woessner J, Wiemer S (2005) Assessing the quality of earthquake catalogues: estimating the magnitude of completeness and its uncertainty. *Bull Seismol Soc Am* 95(2):684–698

Yang Z and Chen WP (2010) Earthquakes along the East African Rift system: a multiscale, system-wide perspective. *J Geophys Res Solid Earth* 115(B12).

ZMAP (2022) <https://github.com/swiss-seismological-service/zmap7/>. Accessed Feb 2022

Publisher's Note Springer Nature remains neutral with regard to jurisdictional claims in published maps and institutional affiliations.